

**IDENTIFICATION AND CHARACTERIZATION OF
HUMAN MEVALONATE KINASE INHIBITORS**

by © Saman Salari

A thesis submitted to the school of graduate studies in partial fulfillment
of the requirements for the degree of

Master of Science

Department of Biochemistry, Faculty of Science

Memorial University of Newfoundland

December 2023

St. John's Newfoundland and Labrador

Abstract

The mevalonate pathway is responsible for the synthesis of isoprenoids, which are essential for various biological activities, such as cell signaling and membrane function. Mevalonate kinase (MK) is a critical enzyme in this pathway, converting mevalonic acid (MVA) to mevalonate-5-phosphate (M-5-P) with ATP as a phosphoryl donor. Mutations in the *MVK* gene, which encodes MK, can cause mevalonate kinase deficiency, an inborn error of metabolism characterized by severe, recurrent inflammation. Previous research has shown that farnesyl pyrophosphate (FPP), a downstream metabolite of the mevalonate pathway, inhibits MK by blocking its ATP binding site. Interestingly, FPP also inhibits FPP synthase, the enzyme that produces FPP. These observations provide evidence for multilayered regulation of the mevalonate pathway, where the single feedback inhibitor FPP targets multiple enzymatic steps. In this thesis, I verified the hypothesis that analogs of FPP that can inhibit FPP synthase could also inhibit MK. Using an enzyme-coupled spectrophotometric assay, I identified several phosphonate compounds that can inhibit MK with nanomolar potency. Further analysis revealed features of these compounds that correlate with their inhibitory activity. The mode of inhibition was also determined for representative compounds. To better understand how MK interacts with its ligands, I have commenced X-ray crystallography studies. The inhibitor compounds identified in this study may serve as a useful tool for future research, for example, in evaluating MK as a new therapeutic target and advancing our understanding of mevalonate pathway regulation.

Acknowledgments

I want to extend my sincere thanks to everyone who played a role in helping me complete this research:

- My supervisor, Dr. Jaeok Park, deserves special mention for his patience and consistent support, both personally and academically. He always reminded me that the pursuit of perfection is a lifelong journey and encouraged me to focus on doing my best instead.
- I am grateful to my supervisor committee members, Dr. Valerie Booth and Dr. Shyamchand Mayengbam, who provided unwavering support whenever I needed.
- Profound thanks to my family, Reza, Gohar, Saman, and Setareh. Despite the miles between us, their encouragement and belief in me have been a source of strength.
- My gratitude extends to my amazing labmates in the Park lab, Vishal, Sean, and Naomi. Their friendship, shared laughter, and assistance with my research were huge support throughout this journey. They made our lab a fun and productive place to be.
- Lastly, my heartfelt appreciation goes to my partner and best friend, Shahab, for being my support during this study. His presence made the tough times easier to bear.

Table of content

Abstract.....	ii
Acknowledgments	iii
Table of content.....	iv
List of Tables	vii
List of Figures.....	viii
List of Abbreviations	ix
Chapter 1: Introduction	1
1.1 Mevalonate pathway	1
1.1.1 Significance of isoprenoids.....	1
1.1.2 Enzymes of the mevalonate pathway.....	1
1.1.3 Dysregulation of the mevalonate pathway and pathological implications	4
1.1.4 Drugs targeting the mevalonate pathway.....	5
1.2 Mevalonate kinase (MK)	6
1.2.1 MK deficiency: clinical and molecular insights	6
1.2.2 Structure of human MK	7
1.2.3 Inhibition of MK	8
1.3 Mevalonate pathway regulation: a multilayered mechanism.....	9
1.3.1 Product inhibition of FPP synthase and GGPP synthase	9
1.3.2 FPP synthase as a cancer target	10
1.3.3 Phosphonate inhibitors of FPP synthase	10
1.4 Research gap and rationale	11
1.5 Hypothesis.....	12

1.6 Objectives	12
Chapter 2. Methodology	14
2.1 Construction of expression vector	14
2.2 Transformation of bacterial host.....	14
2.3 Expression of MK.....	14
2.4 Batch binding purification	15
2.5 Large-scale purification of MK	16
2.6 Enzyme-coupled MK assay	17
2.7 Kinetic characterization of MK	17
2.8 Inhibitor screening	18
2.9 IC_{50} determination.....	19
2.10 Mode of inhibition and K_i determination.....	19
2.11 Crystallization trials	20
2.12 Molecular docking	20
Chapter 3. Results.....	22
3.1 Expression of MK.....	22
3.2 Purification of MK.....	23
3.3 Kinetic characterization of MK	25
3.4 Inhibition studies.....	28
3.4.1 Identification of potential MK inhibitors.....	28
3.4.2 Inhibition of reporter reactions	33
3.4.3 IC_{50} determination.....	35
3.4.4 Mode of inhibition and K_i determination.....	36

3.5 Crystallization studies	38
3.6 Computational investigation of MK ligand binding	39
Chapter 4. Discussion	44
4.1 Creation of expression vector	44
4.2 Protein expression conditions	46
4.3 Enzyme-coupled MK assay	46
4.4 Characterization of human MK inhibitors	48
4.5 Characterization of inhibitor binding.....	50
4.5.1 Limitations of molecular docking.....	50
4.5.2 Strategies for future crystallographic studies.....	51
Chapter 5. Conclusion	53
Bibliography	54
Appendix I. Supplemental information	63
Appendix II. BioRender’s Publication License	69

List of Tables

Table 1. Structures of bisphosphonate compounds tested in this study.....	29
Table 2. Structures of monophosphonate compounds tested in this study.	30
Table 3. Structures of sulfonylaminophosphonate compounds tested in this study.	32
Table 4. IC_{50} of FPP and phosphonate inhibitors for MK inhibition.....	35
Table 5. Free energy of binding for MK ligands calculated by AutoDock Vina.....	43
Table S1. The Classics Suite composition.....	63
Table S2. The PEGs Suite composition.....	65
Table S3. The AmSO4 Suite composition.....	67

List of Figures

Figure 1. Schematic representation of the human mevalonate pathway.....	3
Figure 2. Molecular structures of isoprenoid intermediates.	4
Figure 3. Crystal structure of human MK (PDB ID 2R3V).....	8
Figure 4. SDS-PAGE analysis of MK expression under different conditions.....	23
Figure 5. Purification of MK by size-exclusion chromatography.	24
Figure 6. Estimated molecular weight of MK.	25
Figure 7. Standard curve for NADH absorbance at 340 nm.....	26
Figure 8. Steady-state kinetics of human MK.	27
Figure 9. Inhibition of enzyme-coupled MK reaction by phosphonate compounds.....	33
Figure 10. Effects of MK inhibitors on MK-omitted coupled enzyme reaction.....	34
Figure 11. Dose-response curves for IC ₅₀ determination.....	35
Figure 12. Steady-state kinetic analysis of MK inhibition by phosphonate compounds.....	37
Figure 13. Crystals formed under different crystallization conditions.	39
Figure 14. Binding poses of MK ligands as predicted by AutoDock Vina.	41
Figure 15. Correlation analysis between measured IC ₅₀ and predicted binding energy of MK inhibitors.	42
Figure 16. Amino acid sequence annotation of recombinant human MK.	45
Figure 17. Schematic overview of the pyruvate kinase-lactate dehydrogenase-coupled assay for measuring MK activity.	47
Figure 18. Structural determinants of inhibition potency.	49
Figure S1) Publication permission for Figure 1.....	69
Figure S2) Publication permission for Figure 17.....	70

List of Abbreviations

ADP	Adenosine diphosphate
ATP	Adenosine triphosphate
EDTA	Ethylenediaminetetraacetic acid
FPP	Farnesyl pyrophosphate
GPP	Geranyl pyrophosphate
GTPase	Guanosine triphosphatase
GGPP	Geranylgeranyl pyrophosphate
HEPES	4-(2-hydroxyethyl)-1-piperazineethanesulfonic acid
His-tag	Polyhistidine-tag
HMG-CoA	3-hydroxy 3-methylglutaryl coenzyme A
IPP	Isopentenyl pyrophosphate
IPTG	Isopropyl- β -D-1-thiogalactoside
LB	Lysogeny broth
M-5-P	Mevalonate-5-phosphate
MK	Mevalonate kinase
MVA	Mevalonic acid
N-BP	Nitrogen-containing bisphosphonate
NAD ⁺	Oxidized nicotinamide adenine dinucleotide
NADH	Reduced nicotinamide adenine dinucleotide
OD ₆₀₀	Optical density at 600 nm
PEG	Polyethylene glycol

RMSD	Root-mean-square deviation
SDS-PAGE	Sodium dodecyl sulfate polyacrylamide gel electrophoresis
SOC	Super optimum medium with catabolic repressor
TEV	Tobacco etch virus

Chapter 1: Introduction

1.1 Mevalonate pathway

The mevalonate pathway is an essential biochemical pathway responsible for synthesizing a group of molecules known as isoprenoids. Isoprenoids include a wide array of compounds critical for various biological processes, such as cell signaling, maintenance of cellular membrane structure and function, and the biosynthesis of key molecules like cholesterol, ubiquinone, and steroid hormones (Sacchettini & Poulter, 1997).

1.1.1 Significance of isoprenoids

Isoprenoids play important roles in numerous cellular processes, each with unique significance. Cholesterol, for example, is an essential component of cellular membranes that directly influences their fluidity (Chabanel et al., 1983). Its presence ensures that cells maintain their structural integrity and function optimally. Additionally, cholesterol serves as the precursor for the synthesis of steroid hormones and vitamin D, which are essential for maintaining calcium homeostasis and bone health (Khosla & Monroe, 2018; Veldurthy et al., 2016). Ubiquinone, also known as coenzyme Q, functions as a cofactor in cellular energy generation. It facilitates Adenosine triphosphate (ATP) production by participating in the electron transport chain, supporting the energy demands of cellular activities (Crane et al., 1957). In addition to its role in energy production, ubiquinone also serves as an antioxidant. Its capacity to neutralize harmful reactive oxygen species protects cells from oxidative damage, thereby safeguarding cellular health and longevity (Popov et al., 2001).

1.1.2 Enzymes of the mevalonate pathway

The mevalonate pathway initiates with acetyl-coenzyme A (acetyl-CoA) as the precursor molecule and yields two products, isopentenyl pyrophosphate (IPP) and dimethylallyl

pyrophosphate (DMAPP), which serve as building blocks for the synthesis of more complex downstream isoprenoid metabolites (Figure 1; see Figure 2 for IPP and DMAPP structures). The mevalonate pathway can be divided into two distinct phases: the upper mevalonate pathway and the lower mevalonate pathway. In the upper mevalonate pathway, two acetyl-CoA molecules undergo condensation, resulting in the formation of acetoacetyl-CoA. Subsequently, another condensation step leads to the production of 3-hydroxy-3-methyl-glutaryl-CoA (HMG-CoA). The following reduction of HMG-CoA to mevalonic acid (MVA) represents a rate-limiting, regulatory step. Catalyzed by HMG-CoA reductase, this step ensures a controlled, balanced synthesis of MVA (Durr & Rudney, 1960).

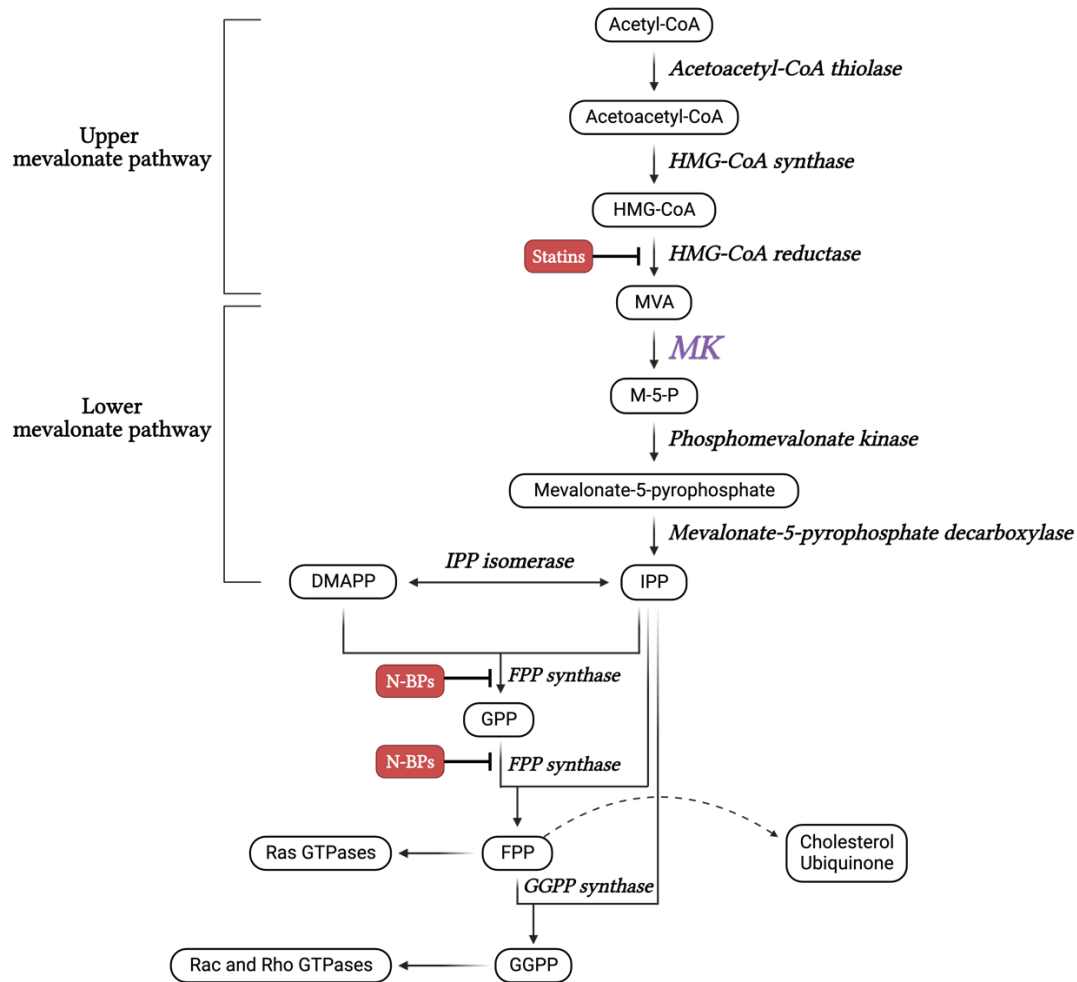


Figure 1. Schematic representation of the human mevalonate pathway. The mevalonate pathway ends with the production of IPP and DMAPP in its strict definition but is commonly extended to include the production of FPP and GGPP. Drugs targeting the pathway enzymes are shown in red. Abbreviations: M-5-P, mevalonate-5-phosphate; N-BPs, nitrogen-containing bisphosphonates; GPP, geranyl pyrophosphate; FPP, farnesyl pyrophosphate; GGPP, geranylgeranyl pyrophosphate; GTP, guanosine triphosphate. Created with BioRender.com.

Following the mevalonate pathway, a head-to-tail condensation of IPP and DMAPP produces geranyl pyrophosphate (GPP). GPP is then elongated through additional condensations with IPP to farnesyl pyrophosphate (FPP) and geranylgeranyl pyrophosphate (GGPP) (Figure 1; see Figure 2 for FPP and GGPP structures). FPP serves as the precursor for all downstream isoprenoid metabolites, including cholesterol and ubiquinone. Additionally, FPP, along with

GGPP, is used as the prenyl group donor in the post-translational modification of membrane-targeted proteins, such as small guanosine triphosphatase (GTPases). Known as prenylation, this process is essential for anchoring these proteins to cellular membranes, enabling their participation in various cellular signaling processes, for example, for cell growth and differentiation (Hooff et al., 2010; McTaggart, 2006).

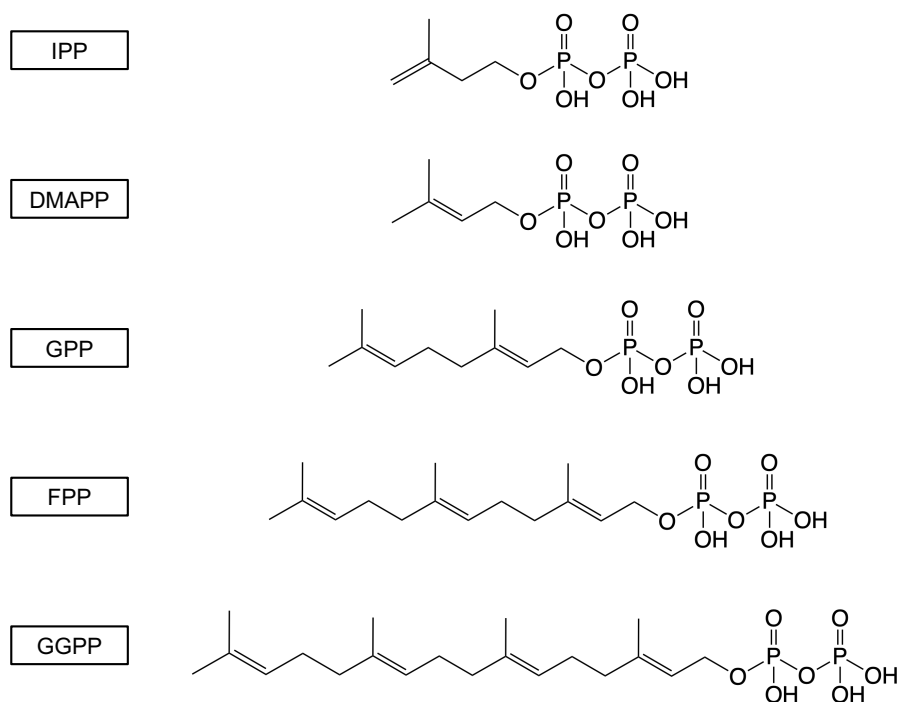


Figure 2. Chemical structures of isoprenoid intermediates. Abbreviations: IPP, isopentenyl pyrophosphate; DMAPP, dimethylallyl pyrophosphate; GPP, geranyl pyrophosphate; FPP, farnesyl pyrophosphate; GGPP, geranylgeranyl pyrophosphate. Structure images were created with the ChemDraw software.

1.1.3 Dysregulation of the mevalonate pathway and pathological implications

Since the mevalonate pathway is essential for the biosynthesis of isoprenoids, dysregulation of this pathway has critical implications in diseases. (i) Cardiovascular diseases: dysregulation of the mevalonate pathway can lead to an excessive production of cholesterol, resulting in the accumulation of low-density lipoprotein (LDL) cholesterol in blood vessels

(Faulkner & Jo, 2022). Elevated levels of LDL cholesterol are a well-established risk factor for cardiovascular diseases, such as atherosclerosis (Graham et al., 2012). (ii) Neurodegenerative disorders: dysregulation of the mevalonate pathway can disrupt cholesterol homeostasis in the brain, leading to elevated brain cholesterol levels. High levels of brain cholesterol can promote the production and aggregation of amyloid beta peptides (Refolo et al., 2000), which contribute to the pathogenesis of Alzheimer's disease by forming toxic aggregates (Vardy et al., 2005). (iii) Cancer: the mevalonate pathway is essential for protein prenylation and is thus required for the proper functioning of Ras and Rho GTPases (Casey, 1992). Dysregulation of this pathway can lead to the overactivation of small GTPases, triggering signaling pathways to promote uncontrolled cell growth and division. This uncontrolled cell proliferation is a hallmark of various cancers, including breast cancer (Fritz et al., 2002).

1.1.4 Drugs targeting the mevalonate pathway

Owing to its essential role in cellular metabolism, the mevalonate pathway has been an important point of pharmacological intervention. The drugs targeting this pathway treat conditions associated with the pathologies discussed above. Two blockbuster classes of drugs stand out (Figure 1). (i) Statins: a class of drugs developed to lower blood cholesterol levels by inhibiting HMG-CoA reductase (Endo, 1992). This inhibition also increases the number of LDL receptors on cell surfaces, with the enhanced receptor activity leading to further reduction in cardiovascular risk (Farmer & Gotto, 1996). (ii) Nitrogen-containing bisphosphonates (N-BPs): a class of drugs used to treat bone-resorption disorders, such as osteoporosis (Rogers et al., 2020). They function by inhibiting FPP synthase, which results in the depletion of FPP and GGPP. Consequent downregulation of protein prenylation, including that of small GTPases, disrupts signaling pathways involved in cell survival, leading to apoptosis in affected cells (Luckman et al., 1998).

1.2 Mevalonate kinase (MK)

MK is an ATP-dependent enzyme responsible for catalyzing the phosphorylation of mevalonate, converting it to mevalonate-5-phosphosphate (M-5-P) (Miziorko, 2011). MK is a member of the GHMP kinase family, a group of enzymes involved in various metabolic pathways which are ATP-dependent enzymes. The acronym GHMP derives from the initial letters of its founding constituents: galactokinase, homoserine kinase, mevalonate kinase, and phosphomevalonate kinase (Bork et al., 1993).

1.2.1 MK deficiency: clinical and molecular insights

Mevalonate kinase deficiency is a rare, recessively inherited autoinflammatory disorder with a spectrum of phenotypic manifestations (Favier & Schulert, 2016). This disorder emerges from disruption in the function of MK due to genetic mutations. These mutations primarily affect the *MVK* gene, which encodes MK. Without properly functioning MK, the mevalonate pathway is compromised, leading to a cascade of detrimental downstream effects. Mevalonate kinase deficiency exhibits three distinct clinical phenotypes. (i) Hyper-immunoglobulin D (IgD) syndrome: hyper-IgD syndrome represents a milder form of mevalonate kinase deficiency (Houten et al., 2003). Individuals afflicted with this condition experience recurrent fever episodes, often accompanied by elevated IgD levels (Drenth et al., 1994). Alongside recurrent fevers, patients may report abdominal pain, joint pain, and skin rashes (Van Der Meer et al., 1984). (ii) Mevalonic aciduria: mevalonic aciduria is the severe type of mevalonate kinase deficiency that is a serious metabolic disease. It is characterized by profound and debilitating symptoms, including developmental delays, intellectual disability, failure to thrive, muscle weakness, and progressive neurological deficits (Hoffmann et al., 1993, 2009). (iii) Disseminated superficial actinic porokeratosis: this more recently discovered phenotype is completely different from the systemic diseases. It is a relatively rare skin condition characterized by the development of multiple small,

raised, scaly patches on the skin's surface (Zhang et al., 2012). While there is no cure for these diseases, the approach to managing mevalonate kinase deficiency primarily focuses on alleviating symptoms and enhancing the overall quality of life for individuals affected by the condition (Van Der Hilst et al., 2008).

1.2.2 Structure of human MK

Human MK is a protein composed of 396 amino acids with a molecular mass of 42,451 Da. The apo-structure of human MK was determined at a resolution of 2.5 Å (Fu et al., 2008) and is accessible in the Protein Data Bank (PDB) under the entry code 2R3V (Figure 3). The N-terminal domain, spanning amino acids 1 to 229 and 373 to 396, is characterized by eight-stranded β sheet packed with seven α -helices. The C-terminal domain, with amino acids 230 to 344, consists of five α -helices and four β strands. As a kinase enzyme, MK is ATP-dependent and possesses a cofactor binding site composed of residues Ser146, Glu193, His197, and Asp204. An Mg^{2+} ion is expected to bind here to facilitate ATP binding and hydrolysis during catalysis. Currently, there are no other crystal structures of human MK available, and therefore, its binding interactions with substrates or other ligands have not been directly elucidated.

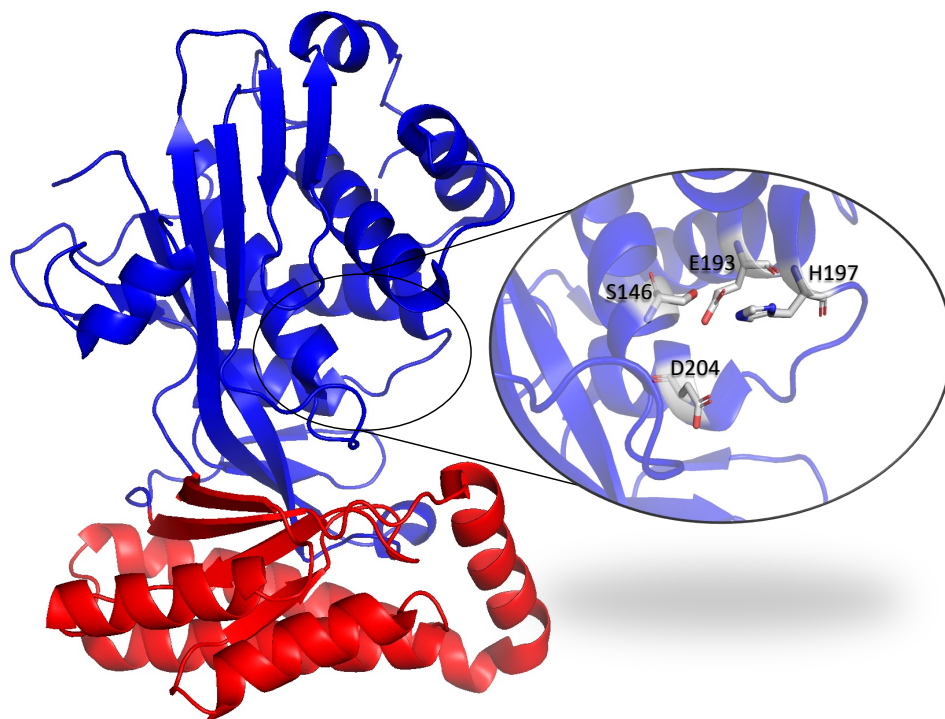


Figure 3. Crystal structure of human MK (PDB ID 2R3V). The N-terminal domain is highlighted in blue, and the C-terminal domain in red. The residues involved in the cofactor binding is indicated in a stick representation. The molecular visualization software PyMOL was used to create the image.

1.2.3 Inhibition of MK

The inhibition of MK by various isoprenoid intermediates, including IPP, DMAPP, FPP, and GGPP has been previously reported (Dorsey & Porter, 1968; Hinson et al., 1997). All of these compounds were found to act competitively with ATP. Notably, FPP and GGPP are the most potent inhibitors, characterized by low inhibition constants (K_i) of 10–104 nM and 59 nM, respectively (Fu et al., 2008; Hinson et al., 1997; Potter & Mizioroko, 1997). In contrast, DMAPP and IPP were shown to be weaker inhibitors, with higher K_i values of 16 μ M and 20 μ M, respectively (Hinson et al., 1997). The inhibition of MK by the isoprenoid intermediates has broader implications for the regulation of the mevalonate pathway, as described below.

1.3 Mevalonate pathway regulation: a multilayered mechanism

The mevalonate pathway is intricately controlled by a complex web of feedback regulation. The control mechanism involves downregulating enzymatic steps at both the transcriptional and protein levels, in response to the accumulation of downstream metabolites and those within the pathway. For example, high levels of cholesterol result in decreased expression and increased degradation of HMG-CoA, the gate-keeper enzyme of the pathway (Goldstein & Brown, 1990). Within the pathway, as described above, FPP and GGPP can inhibit the upstream enzyme MK. Furthermore, FPP and GGPP can inhibit the enzymes responsible for their immediate production, namely, FPP synthase (Park, Zielinski, et al., 2017) and GGPP synthase (Kavanagh et al., 2006). The multilayered control mechanism functions to minimize the risk of uncontrolled isoprenoid synthesis, which could lead to cellular dysfunction and disease. The convergence of feedback inhibition at different stages of the pathway underscores the tight coordination between metabolic flux and cellular requirements. This intricate regulation mechanism ensures that isoprenoid synthesis remains responsive to both internal and external factors, allowing cells to efficiently adapt to varying physiological demands (Kang & Lee, 2016).

1.3.1 Product inhibition of FPP synthase and GGPP synthase

Two examples of feedback inhibition in the mevalonate pathway involve self-inhibition of enzymes by their own catalytic products. (i) Inhibition of FPP synthase by FPP: this inhibition occurs through an allosteric mechanism. FPP binds to an allosteric site, triggering a conformational change that locks the enzyme into a non-catalytic state (Park, Zielinski, et al., 2017). This mechanism allows for the rapid downregulation of FPP synthase activity without compromising the enzyme's inherent catalytic efficiency. (ii) Inhibition of GGPP synthase by GGPP: GGPP synthase undergoes a similar process of self-inhibition. However, the mechanism here is different; GGPP functions as a competitive inhibitor. While a large portion of GGPP binds into a pocket

outside the enzyme's active site, the pyrophosphate head group of GGPP still binds to the enzyme's active site (Kavanagh et al., 2006). The affinity of these product feedback interactions is in the low micromolar range, with the dissociation constants (K_d/K_i) of 5 μM and 25 μM for the FPP-FPP synthase and GGPP-GGPP synthase complexes, respectively (Kavanagh et al., 2006; Park, Zielinski, et al., 2017).

1.3.2 FPP synthase as a cancer target

As mentioned previously, FPP is essential for the prenylation of signaling proteins, including the small GTPases involved in cell migration and invasion (Wang & Casey, 2016). Inhibiting FPP synthase, which leads to reduced FPP levels, can consequently downregulate these cellular processes. This property makes FPP synthase an attractive target for cancer therapy, especially in cases of metastatic cancers. Additionally, FPP synthase plays a key role in the biosynthesis of cholesterol and other essential isoprenoids. Cancer cells often exhibit an elevated demand for these metabolites to support their rapid growth and uncontrolled division (Kuzu et al., 2016). By inhibiting FPP synthase, it may be possible to deprive cancer cells of these critical metabolites, thereby impeding their growth and proliferation (Aparicio et al., 1998; Boissier et al., 1997; Shipman et al., 1997). Furthermore, the inhibition of FPP synthase can be integrated into combination therapies with other cancer treatments, such as chemotherapy or targeted therapies. Therefore, targeting FPP synthase in cancer therapy holds great promise due to its ability to disrupt processes involved in cancer cell growth and survival. This approach is considered a compelling avenue for developing novel therapeutic strategies against different types of cancer (Berndt et al., 2011; Mullen et al., 2016).

1.3.3 Phosphonate inhibitors of FPP synthase

Phosphonate inhibitors of FPP synthase have been investigated for their applications in treating a spectrum of medical conditions, including lytic bone diseases, metabolic disorders like

osteoporosis, and specific types of cancer such as multiple myeloma, breast cancer, and prostate cancer (Berndt et al., 2011). As discussed earlier, the bisphosphonate drugs N-BPs are currently used in clinical practice to treat bone-resorption disorders, including osteoporosis. Their mechanism of action involves the inhibition of FPP synthase and the resulting disruption of protein prenylation, especially affecting small GTPases (Rogers et al., 2020). Clinical evidence underscores the anticancer therapeutic potential of N-BPs (Morgan et al., 2010; Pazianas et al., 2012; Valachis et al., 2013); however, they suffer from limitations such as poor distribution and limited cellular uptake in non-skeletal tissues.

Other phosphonate inhibitors of FPP synthase explored for their therapeutic potential include thienopyrimidine-based monophosphonate compounds (Feng et al., 2019; Park, Leung, et al., 2017). Designed as structural analogues of FPP, these compounds inhibit FPP synthase via the same mechanism as FPP: by binding to the allosteric site and locking the enzyme in an inactive conformation. Notably, these compounds have been investigated as drug candidates for non-skeletal forms of cancer. However, developing clinically applicable allosteric inhibitors of FPP synthase has proven challenging. Most of the inhibitors tested so far demonstrated potency in the micromolar range, which makes them unsuitable for clinical use, with the most potent compound showing an IC_{50} value of 0.54 μM (Feng et al., 2019). This outcome aligns with the fact that FPP inhibits FPP synthase with micromolar potency ($K_d \sim 5 \mu\text{M}$) (Park, Zielinski, et al., 2017).

1.4 Research gap and rationale

Despite its central role in isoprenoid biosynthesis, our understanding of MK remains limited, both in its structural characteristics and functional implications. Currently, only one structure of human MK is available, and information regarding its interactions with substrates or potential ligands is scarce. Structures of human MK in complex with various ligands or in different

conformational states would greatly enhance our understanding of its catalytic mechanism and possible interactions with small molecules that could modulate its activity. It is important that the mevalonate pathway is a current clinical target. As mentioned above, inhibitors of HMG-CoA reductase and FPP synthase are used as treatments for hypercholesterolemia and bone resorption disorders. Notably, both these enzymes play roles in the feedback regulation of the mevalonate pathway. However, the clinical utility of MK, another key player in mevalonate pathway regulation, remains unknown. In this context, the fact that inhibiting the mevalonate pathway produces anticancer effects, and clinically relevant molecules capable of this action have yet to be identified, is of special interest. If small molecule inhibitors of MK were to become available, it would be possible to investigate MK as a potential target for anticancer drug development. Therefore, this thesis aims to address the knowledge gaps related to MK's structure and function, particularly concerning its potential as a drug target.

1.5 Hypothesis

I hypothesize that the FPP-mimicking phosphonate compounds designed to inhibit FPP synthase will also inhibit MK. Since FPP exhibits more than a 100-fold greater inhibitory activity against MK than FPP synthase, I anticipate that these compounds will also demonstrate greater inhibitory activity against MK than against FPP synthase.

1.6 Objectives

This thesis is guided by the following specific objectives:

- (i) Identification of MK inhibitors: the primary goal is to discover novel inhibitors of MK by screening previously synthesized phosphonate inhibitors of FPP synthase *in vitro*.
- (ii) Characterization of MK inhibitors: if such inhibitors are discovered, I will examine their potency and mechanism of action through detailed kinetic analysis.

(iii) Structural investigation of MK-ligand binding: I aim to elucidate structures of human MK in complex with its substrates and inhibitors using X-ray crystallography.

These objectives collectively aim to advance our knowledge of MK, its potential inhibitors, and the molecular interactions governing its function. The findings from this research will lay the groundwork for future studies that will further our understanding of mevalonate pathway regulation and provide potential avenues for therapeutic intervention related to this pathway.

Chapter 2. Methodology

2.1 Construction of expression vector

To create an expression vector encoding human MK (UniProt Q03426), its cDNA sequence was optimized for *E. coli* codons, and a corresponding DNA fragment was chemically synthesized. The DNA was cloned into the pET-15b plasmid through the NdeI and XhoI sites, in frame with the sequence encoding a polyhistidine-tag (His-tag) and a thrombin cleavage site preceding the restriction sites. This work was outsourced to GenScript, who provided 4 µg of sequence-verified, lyophilized plasmid DNA as the final product.

2.2 Transformation of bacterial host

E. coli BL21(DE3) competent cells were purchased from New England BioLabs. The plasmid DNA was dissolved in ultrapure Milli-Q water at 50 ng/µL concentration. Transformation was achieved through a heat shock method. Fifty microlitres of the competent cells were combined with 2 µL of the plasmid in an Eppendorf tube and incubated on ice for 10 minutes. The cells were subjected to a brief heat shock through incubation in a water bath at 42 °C for 10 seconds. After the heat shock, the tube was returned to ice and incubated for additional 5 minutes. Nine hundred fifty microlitres of Super Optimal broth with Catabolite repression (SOC) media was added to the tube, which was then incubated at 37 °C for 1 hour with agitation at 200 rpm. Following the incubation, 25 µL of the outgrowth culture were spread onto a lysogeny broth (LB) agar plate supplemented with 100 µg/mL ampicillin. For colony growth, the plate was incubated overnight at 37 °C.

2.3 Expression of MK

A starter culture was established by inoculating 50 mL of LB media containing 100 µg/mL ampicillin with cells from a single colony on the previously prepared agar plate. After overnight

incubation at 37 °C with agitation at 180 rpm, 10 mL of the starter culture were added to 1 L of fresh LB containing the same concentration of ampicillin. The diluted culture was further incubated at 37 °C, shaken at 180 rpm, until its optical density, OD₆₀₀ reached 0.6. Induction of MK expression was initiated by adding 1 mL of 0.1 M isopropyl-β-D-1-thiogalactoside (IPTG) to the culture. Two different induction conditions were tested for optimal expression: 6 hour incubation at 37 °C and overnight incubation at 26 °C. Since no differences were observed in expression efficiency between the two conditions, all subsequent expression experiments were carried out at 37 °C. Cells from each 1 L culture were pelleted separately by centrifugation at 5,000 × g for 10 minutes at 4 °C and then stored at -20 °C.

2.4 Batch binding purification

Two hundred microlitres of Ni-nitrilotriacetic acid agarose resin (Qiagen) were pipetted into each Eppendorf tube. After centrifugation at 0.5 × g for 5 minutes, the supernatant, which contained the manufacturer storage buffer, was discarded. Subsequently, the resin was thoroughly washed with Milli-Q water and then a binding buffer (0.1 M Tris (pH 6.8) and 0.5 M NaCl) to ensure proper equilibration. This equilibration process involved multiple rounds of resin resuspension, centrifugation, and supernatant removal. To prepare cell lysates, 200 mg of cell pellets from the protein expression experiments were resuspended and sonicated in 400 μL of the binding buffer until transparency was achieved. After clarification through centrifugation at 10,000 × g for 10 minutes at 4 °C, the lysates were combined with the pre-equilibrated resin and incubated at room temperature for 1 hour. Subsequently, the resin was centrifuged at 0.5 × g for 5 minutes to isolate the supernatant as the flow-through fraction. To ensure effective removal of unbound proteins, the resin underwent two consecutive washes, each involving the addition of 400 μL binding buffer, followed by a 5 minute incubation, centrifugation, and supernatant aspiration step.

Elution was achieved by adding 400 μ L of a buffer containing 0.1 M Tris (pH 6.8), 0.5 M NaCl, and 0.5 M imidazole, followed by a 5 minute incubation, centrifugation, and supernatant aspiration step. The elution process was repeated once. The resulting supernatants from both the washing and elution steps were analyzed by sodium dodecyl sulfate polyacrylamide gel electrophoresis (SDS-PAGE).

2.5 Large-scale purification of MK

Four cell pellets were used to produce one batch of purified MK. The pellets were resuspended in 200 mL of a loading buffer (50 mM HEPES (pH 7.5), 0.5 M NaCl, 5 mM imidazole, 2 mM β -mercaptoethanol, and 5% glycerol), supplemented with four protease inhibitor cocktail tablets (cOmplete, Roche). The cells were lysed by sonication in cycles of 10-second pulse-on and 20-second pulse-off for the total duration of 30 minutes. The lysate was clarified by centrifugation at $18,000 \times g$ for 90 minutes, followed by syringe filtration through a 0.45 μ m polyvinylidene fluoride membrane (MilliporeSigma). The cleared lysate was passed through a Ni-affinity chromatography column (HisTrap High Performance 5 mL, Cytiva), which was then washed with a wash buffer (50 mM HEPES (pH 7.5), 0.5 M NaCl, 75 mM imidazole, 2 mM β -mercaptoethanol, and 5% glycerol) until no protein eluted. Finally, MK was eluted with an elution buffer containing a higher concentration of imidazole (50 mM HEPES (pH 7.5), 0.5 M NaCl, 0.35 M imidazole, 2 mM β -mercaptoethanol, and 5% glycerol).

To further purify the protein, the eluant from the Ni-affinity purification step was applied to a size exclusion chromatography column (HiLoad Superdex 200 Preparation Grade 16/600, Cytiva). The protein was eluted in a running buffer composed of 10 mM HEPES (pH 7.5), 0.5 M NaCl, 2 mM β -mercaptoethanol, and 5% glycerol. Fractions containing MK were confirmed by SDS-PAGE analysis and combined together. Half of the sample was concentrated to 16 mg/mL

by ultrafiltration with a molecular weight cut-off of 50 kDa (for crystallization studies). The other half was diluted to 1 mg/mL concentration in the size exclusion buffer (for enzyme assays). Both samples were flash-frozen in liquid nitrogen and stored at $-80\text{ }^{\circ}\text{C}$ in 100 μL aliquots. The temperature was kept constant at 4°C throughout all purification procedures.

2.6 Enzyme-coupled MK assay

A coupled enzyme assay was used to make all rate measurements in this study. The coupled enzymes pyruvate kinase and lactate dehydrogenase were purchased as a pre-mixed solution in 10 mM HEPES (pH 7.0), 0.1 M KCl, 0.1 mM ethylenediaminetetraacetic acid (EDTA), and 50% glycerol (Sigma-Aldrich). Typically, reactions proceeded in a buffer containing 50 mM HEPES (pH 7.5), 0.1 M KCl, 10 mM MgCl_2 , 0.15 mM phosphoenolpyruvate, and 0.15 mM reduced nicotinamide adenine dinucleotide (NADH), ~ 8 units of pyruvate kinase, ~ 12 units of lactate dehydrogenase, and 0.5 $\mu\text{g}/\text{mL}$ MK. The concentrations of MVA and ATP were varied depending on the experiment. All reactions were carried out at $32\text{ }^{\circ}\text{C}$ in triplicate unless noted otherwise. Each reaction was pre-incubated for 2 minutes and initiated by adding 10 μL of MK (50 $\mu\text{g}/\text{mL}$; diluted from the $-80\text{ }^{\circ}\text{C}$ stock in 50 mM HEPES, pH 7.5). The total volume of each reaction was 1 mL. Reaction progress was continuously monitored by measuring the absorbance at 340 nm for 1 minute, with absorbance readings recorded every 5 seconds. The measured absorbance was equated to product formation by using the absorption coefficient of NADH determined from a calibration curve ($5.4107\text{ cm}^{-1}\text{ mM}^{-1}$; see the Results section). Blank samples contained all reaction components except NADH and MK. For negative control reactions, water was added instead of MK.

2.7 Kinetic characterization of MK

Initial rate experiments were conducted by varying the concentration of one substrate (i.e., either MVA or ATP) in the range of 20 μ M to 5 mM while keeping the other at a fixed concentration of 5 mM. To determine the steady-state kinetic parameters, the measured rate data were fitted to the following equation describing substrate inhibition:

$$v_i = \frac{V_{max}[S]}{K_m + [S] + \frac{[S]^2}{K_i}}$$

Data fitting analysis was performed with the GraphPad Prism software package. Turnover numbers (k_{cat}) were calculated by dividing the maximum velocity (V_{max}) by the molar concentration of MK added to the reactions.

2.8 Inhibitor screening

Potential inhibitor compounds were received as dry powders and dissolved in Milli-Q water to a master stock concentration of 20 mM. To facilitate their dissolution, 1 or 3 equivalents of NaOH were added to convert them into monosodium salt (for monophosphonates) or trisodium salt (for bisphosphonates), respectively. Their ability to inhibit MK was assessed by using the standard coupled enzyme assay (see Section 2.6). Each compound was tested at two different concentrations: 1 μ M and 10 μ M. MVA and ATP were added at concentrations of 0.5 mM and 0.05 mM, respectively. Percent inhibition was calculated by comparing the initial rate of the inhibited reaction to that of a control reaction without any added inhibitor.

Reactions to test for the potential inhibition of the reporter enzymes consisted of the following components: 50 mM HEPES (pH 7.5), 0.1 M KCl, 10 mM MgCl₂, 0.15 mM phosphoenolpyruvate, 0.15 mM NADH, 0.15 mM adenosine diphosphate (ADP), ~8 units of pyruvate kinase, ~12 units of lactate dehydrogenase, and the tested compound when added. The reactions were initiated by adding the pre-mixed solution of pyruvate kinase and lactate

dehydrogenase. The reaction conditions were identical to the standard MK assay, involving a 2 minute pre-incubation followed by a 1 minute reaction at 32 °C. The reaction volume also remained at 1 mL, but each reaction was carried out in duplicate instead of triplicate. Compounds were only tested at concentrations that yielded significant inhibition in the standard MK assay.

2.9 IC_{50} determination

IC_{50} values were determined for compounds that exhibited greater than 50% inhibition at 10 μ M in the screening studies. The standard coupled enzyme assay was employed, using substrate concentrations of 0.5 mM for MVA and 0.05 mM for ATP. Each potential inhibitor was added to the reaction mixture at varying concentrations, typically at nine concentrations spanning a 10,000-fold concentration range. The IC_{50} values were determined by using GraphPad Prism, which fitted the data to the following equation by non-linear regression:

$$Response = Minimum + \frac{Maximum - Minimum}{1 + 10^{(log IC_{50} - [I])^n}}$$

In this equation, the parameters *Maximum* and *Minimum* denote maximum and minimum response, respectively, and n represents the Hill slope, describing the steepness of the fitted curve.

2.10 Mode of inhibition and K_i determination

The standard coupled enzyme assay was used to measure the initial rates of MK in the presence of inhibitors. The concentration of one substrate was varied in the range of 0.05 to 2 mM, while the other substrate was maintained at a constant, saturating concentration of 5 mM. Specifically, when ATP was held at a constant level, MVA was added at concentrations of 0.1, 0.2, 0.5, 1, and 2 mM. Conversely, when MVA was kept at a constant level, ATP was included at concentrations of 0.05, 0.1, 0.2, 0.5, and 1 mM. Each inhibitor was added at four different concentrations in the range of 0 to 600 nM, which were predetermined in a pilot study to ensure a well-distributed set of data points. The acquired data were analyzed by using GraphPad Prism.

Non-linear regression analysis was applied to fit the data to the Michaelis-Menten equations describing different types of enzyme inhibition. The selection of the most appropriate models was determined through the extra sum-of-squares F test (Kutner, 1997).

2.11 Crystallization trials

Crystallization of MK was attempted by using a hanging-drop vapour diffusion method. One microlitre of a protein solution was combined with 1 μ L of a crystallization buffer and placed on a siliconized glass coverslip. The coverslip was then sealed over a reservoir containing 250 μ L of the same crystallization buffer, suspending the protein-containing droplet over the reservoir. The reservoirs and crystallization drops were set up in 24-well format plates. The protein solution contained 10 mg/mL MK and 2 mM MVA. Commercially available screen solutions from the Classics, PEGs, and AmSO₄ Suites (NeXtal) were used as crystallization buffers (for buffer composition, please refer to Appendix I Supplemental Information). The crystallization plates were incubated at room temperature for a period of up to 6 months.

2.12 Molecular docking

The 3D structures of all ligand compounds were generated by using MarvinSketch (Csizmadia & Csizmadia, 1999). The receptor structure (i.e., the 3D model of MK used for virtual docking of ligand compounds) was derived from the PDB entry 2R3V, the crystal structure of MK in an unliganded state. Prior to docking, the receptor structure underwent preprocessing steps, including the addition of hydrogen atoms and removal of crystallographic water molecules. A magnesium ion found to be involved in ligand binding in a reference structure (rat MK-ATP complex; PDB ID 1KVK) was added in. Subsequently, the structure was energy-minimized by using MGLTools (Morris et al., 2009). Docking simulations were carried out with the AutoDock Vina software (Eberhardt et al., 2021). A search grid box, which completely encompassed the ATP

binding site, was generated with a grid spacing of 0.375 Å. The overall dimensions of the grid box were 38 Å × 38 Å × 40 Å. The center point coordinates of the grid box were set to X = 53.483, Y = 3.162, and Z = -27.740. For each ligand, a total of nine distinct binding poses were generated, and the top-scoring pose with the highest estimated binding energy was selected for subsequent visual inspection.

Chapter 3. Results

3.1 Expression of MK

To produce the protein sample required for this study, I transformed *E. coli* BL21(DE3) cells with a pET-15b expression vector encoding an N-terminally His-tagged copy of human MK. Following overnight incubation on an ampicillin-supplemented LB agar plate, 22 individual colonies formed, indicating the successful uptake of the expression vector by the host cells. I selected one of these colonies and expanded it in LB to create an expression culture. The overexpression of the recombinant protein was induced by adding IPTG. Two different incubation conditions were tested to optimize MK expression: one involved incubating the cells at 37 °C for 6 hours, and the other at 26 °C overnight (16 hours).

To quickly validate the presence of the MK protein in my sample, I used batch binding chromatography followed by SDS-PAGE analysis. Batch binding allows for a quick isolation of His-tagged proteins from cell lysates. After batch binding, I used SDS-PAGE to analyze the protein content of my samples. The resulting gels showed a prominent band with a molecular weight of approximately 44 kDa, consistent with the expected molecular weight of MK (Figure 4). There was no obvious difference in the expression levels between the two tested incubation conditions, although the overnight incubation at 26 °C may have yielded slightly higher MK expression. No clear differences were observed in the protein profiles. This result suggests that both conditions were similarly effective in inducing MK expression.

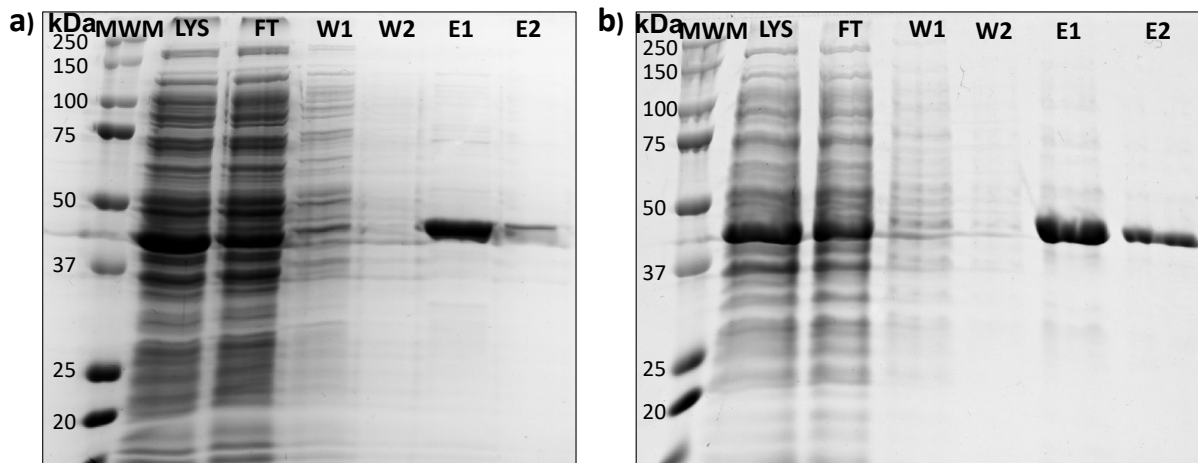


Figure 4. SDS-PAGE analysis of MK expression under different conditions. a) 6-hour expression at 37 °C. b) Overnight expression at 26 °C. Cell lysates derived from the two expression cultures were purified by a batch binding method. An 8% polyacrylamide gel was used to separate the samples. Label abbreviations: MWM, molecular weight marker; LYS, lysate; FT, flow-through; W, wash fractions; E, elution fractions.

For the subsequent, larger scale expression experiment, where I grew four 1 L expression cultures, I proceeded with the 37 °C condition. The choice was based on practical considerations, as this condition allowed for a shorter incubation period, making it more time-efficient while still yielding satisfactory protein production.

3.2 Purification of MK

Purification of MK from the large-scale expression was achieved in two chromatographic steps. After the initial Ni-affinity purification, I used size-exclusion chromatography as the second purification step. Size-exclusion chromatography separates proteins based on their size and shape, and therefore, this second step complements the Ni-affinity purification step, which takes advantage of the protein's affinity to the column matrix conferred by the recombinantly introduced His-tag. The chromatogram from the size-exclusion step showed a clear separation of one large peak at the elution volume of 69 mL from three smaller peaks at 46, 59, and 120 mL (Figure 5a), confirming that this step further purified the Ni-affinity sample.

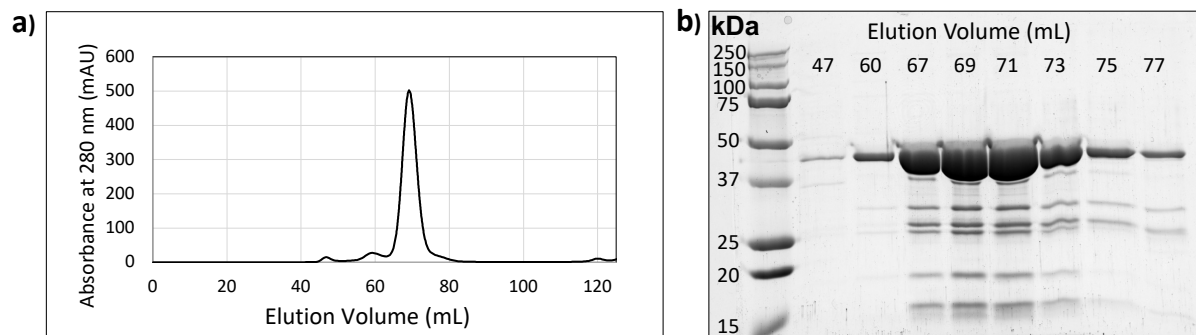


Figure 5. Purification of MK by size-exclusion chromatography. a) Chromatogram from the size-exclusion step. b) SDS-PAGE analysis of the eluant. An 8 % polyacrylamide gel was used to separate the samples.

The eluant from the size-exclusion column was collected as 1 mL fractions. To assess the purity of the eluant, representative fractions were analyzed for their protein content by SDS-PAGE (Figure 5b). Once again, a prominent band with a molecular weight of ~44 kDa was observed, confirming the successful expression and purification of my protein. Impurities in the sample included those in the 25–37 kDa range, which eluted slightly later than MK, possibly explaining the right shoulder on the main peak in the chromatogram. The purity of the collected fractions was further assessed by using the Bio-Rad GelDoc Go System, which estimated a purity of 85% (i.e., MK accounts for 85% of the total protein in the sample), a value generally considered sufficient for enzymatic studies. Fractions corresponding to the centre portion of the size-exclusion peak were pooled into a single batch, yielding a total of 12 mg of protein.

A useful feature of size-exclusion chromatography is its ability to estimate the size of the purified protein in its native, non-denatured state. I estimated the molecular weight of my protein by comparing its elution volume to that of known molecular weight standards (Figure 6a). The experimental molecular weight is approximately double the theoretical molecular weight of the MK monomer (Figure 6b), indicating that MK exists as a dimer in solution. The slight discrepancy

between the experimental value (96,721 kDa) and the theoretical value calculated for a dimer (89,228 kDa) can be attributed to the shape of the MK dimer.

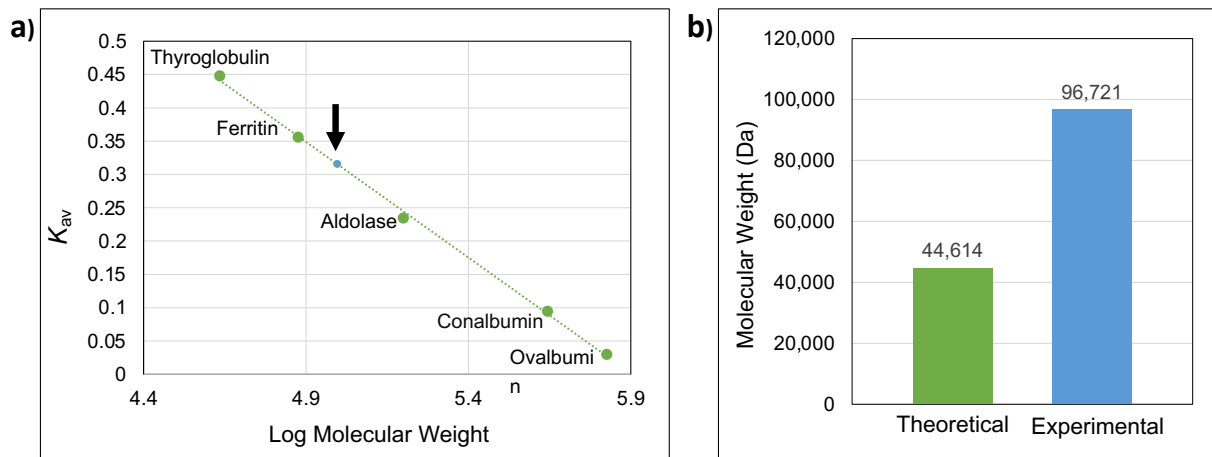


Figure 6. Estimated molecular weight of MK. a) Calibration curve for the chromatographic column used for the size-exclusion step. Green circles represent the standard proteins. Blue circle represents MK. K_{av} (partition coefficient) = (elution volume – void volume) ÷ (column volume – void volume). The calibration curve was previously generated by my thesis supervisor, Dr. Park. b) The theoretical monomer weight of my recombinant MK is represented in green; the molecular weight determined by size-exclusion is shown in blue.

3.3 Kinetic characterization of MK

After obtaining a sufficient amount of purified enzyme for subsequent studies, I proceeded to confirm its catalytic activity. I used a coupled enzyme assay incorporating pyruvate kinase and lactate dehydrogenase (discussed in Section 4.2). Since the assay relied on measuring NADH absorbance, which decreases as NADH is converted to oxidized nicotinamide adenine dinucleotide (NAD^+) in the coupled reaction, I first generated a standard curve correlating NADH concentration with absorbance at 340 nm (Figure 7). From this curve, I determined the absorption coefficient of NADH ($0.5407 \text{ cm}^{-1} \text{ mM}^{-1}$), which I later used to convert the reduction in absorbance into the formation of M-5-P in subsequent experiments.

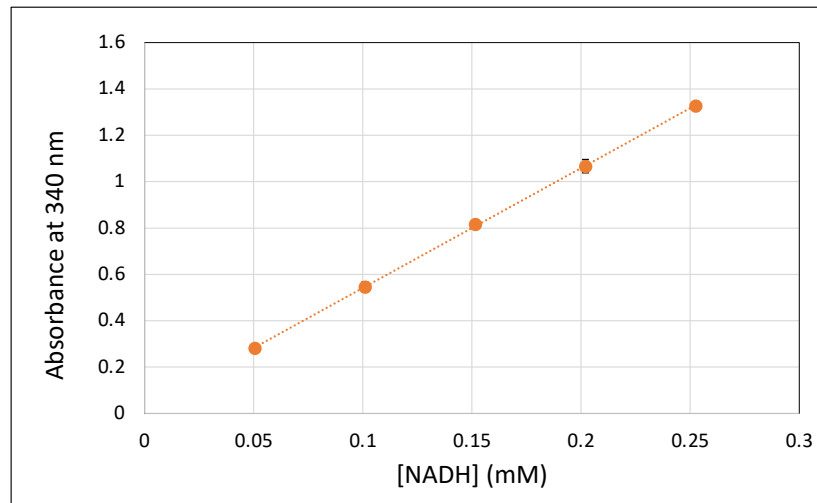


Figure 7. Standard curve for NADH absorbance at 340 nm. Linear regression analysis was applied to generate the curve, the slope of which represents the absorption coefficient of NADH ($0.5407 \text{ cm}^{-1} \text{ mM}^{-1}$). Only the absorbance values < 1 were used for the linear regression. Error bars represent the standard deviation of two independent measurements.

Subsequently, I carried out initial rate experiments to characterize the kinetic behaviour of my recombinant MK protein (Figure 8). As expected for a typical enzyme, the initial rate did not show a linear relationship with substrate concentration. Instead, the initial rate plateaued at higher substrate concentrations, reflecting the enzyme becoming saturated with substrate. Furthermore, as the substrate concentrations continued to increase (i.e., when $[\text{ATP}] > 3 \text{ mM}$ and $[\text{MVA}] > 2 \text{ mM}$), the enzyme demonstrated slightly decreased initial rates, indicating the presence of substrate inhibition. This observation suggests that the enzyme is inhibited by its own substrates under saturating conditions. Therefore, V_{max} , the maximum rate possible for this enzyme-catalyzed reaction, can never be reached under the given substrate conditions.

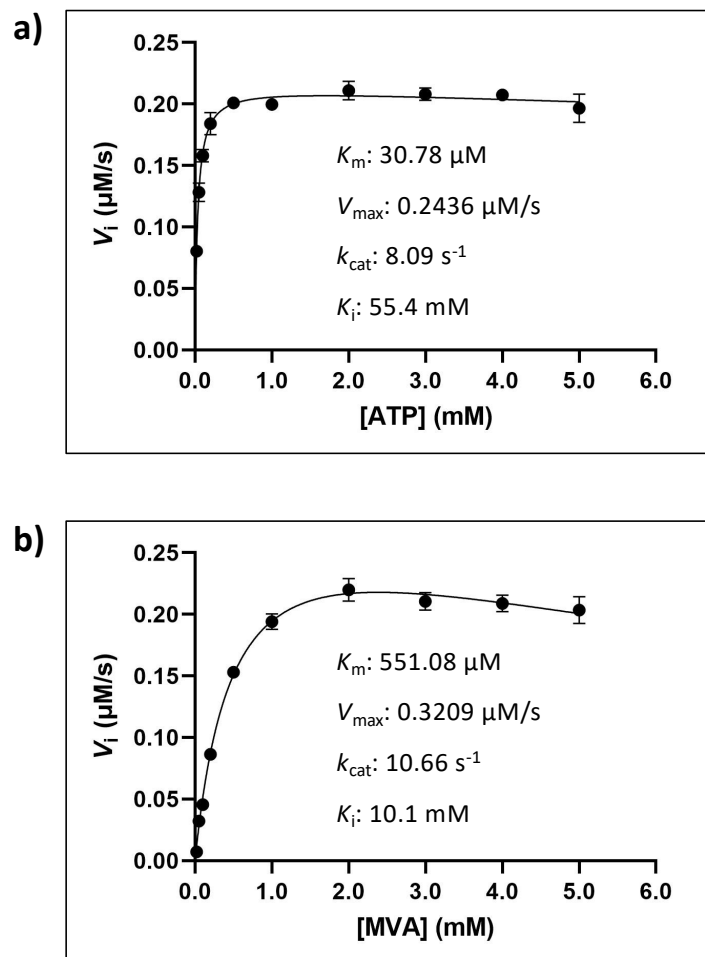


Figure 8. Steady-state kinetics of human MK. a) Plot of initial rates vs. varying concentrations of ATP, determined at a fixed concentration of 5 mM MVA. b) Plot of initial rates vs. varying concentrations of MVA, determined at a fixed concentration of 5 mM ATP. Error bars represent the standard deviation of triplicate experiments. The kinetic parameters determined from each curve are displayed.

To determine the kinetic parameters for the MK catalytic reaction, I fitted the rate data by non-linear regression to a Michaelis-Menten model incorporating substrate inhibition (see Chapter 2 for the equation). To validate the obtained values, I compared them with previously reported data from the literature. The Michaelis-Menten constant (K_m) values closely align with those from previous studies ($K_m^{\text{MVA}} = 41\text{--}150 \mu\text{M}$; $K_m^{\text{ATP}} = 74\text{--}440 \mu\text{M}$) (Fu et al., 2008; Hinson et al., 1997; Potter & Mizioro, 1997), suggesting that I was successful in producing a fully functional recombinant version of MK. However, these studies did not report substrate inhibition in MK. It

is possible that they did not take into consideration the slight decrease in initial rates at saturating concentrations of the substrates; they used the standard Michaelis-Menten model to analyze the data according to their methods sections. However, this cannot be confirmed from the papers alone because they only reported the determined values without showing the actual Michaelis-Menten plots.

The determined kinetic parameters have significant implications for understanding MK's enzymatic behavior. For example, K_m , indicates the substrate concentration at which an enzyme achieves half of its V_{max} . Under steady-state conditions, these values reflect the enzyme's affinity for the substrate, with lower K_m values indicating more efficient enzyme-substrate interactions. Therefore, our data indicate that ATP binds to MK approximately 18-fold more tightly than MVA. The K_i values, representing the substrate inhibition constants, reveal the concentration at which substrates begin to exert significant inhibitory effects on the enzyme (i.e., the concentration required to produce half maximum inhibition). Although both are weak inhibitors, the determined values indicate that MVA has a greater effect as a substrate inhibitor than ATP (11 mM and 85 mM for MVA and ATP, respectively; Figure 8).

3.4 Inhibition studies

3.4.1 Identification of potential MK inhibitors

Having established the functionality of the recombinantly produced MK, I proceeded to explore potential inhibitors of the enzyme. Our collaborators in the Tsantrizos lab (McGill University) provided a collection of 29 synthetic small molecules, originally designed as FPP-mimetics capable of inhibiting FPP synthase (De Schutter et al., 2010, 2012; Leung et al., 2013; Park et al., 2012; Park, Leung, et al., 2017). These molecules represented a diverse panel of phosphonate compounds, including eight bisphosphonates (Table 1), 17 monophosphonates (Table 2), and four sulfonylaminophosphonates (Table 3).

Table 1. Structures of bisphosphonate compounds tested in this study. Chemical structures were created with ChemDraw.

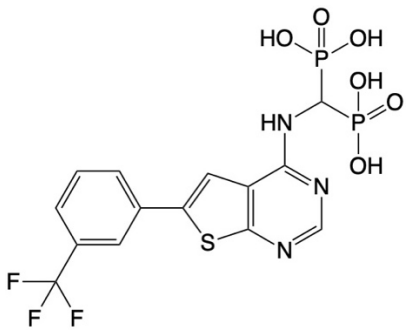
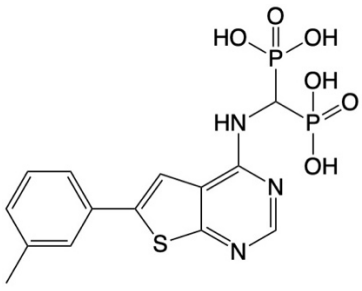
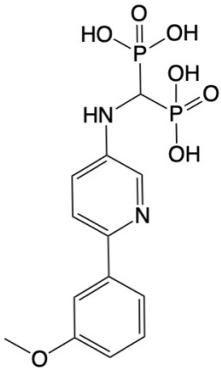
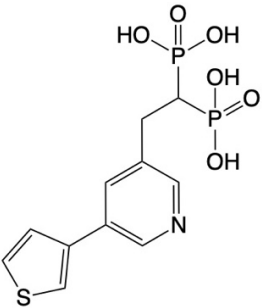
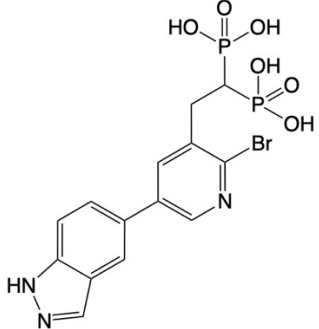
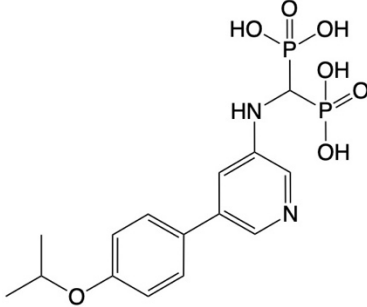
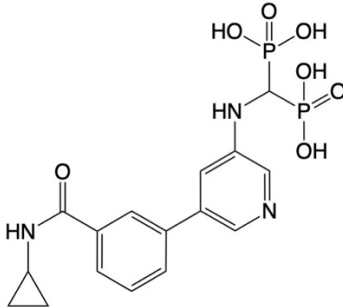
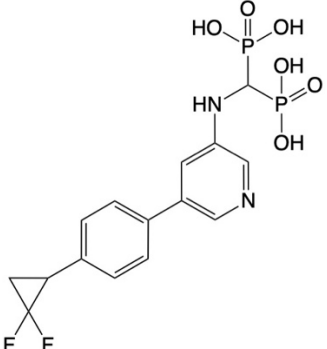
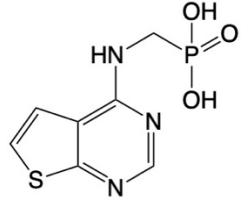
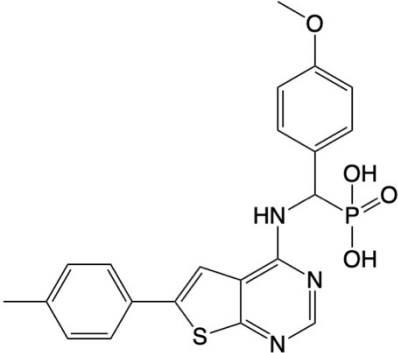
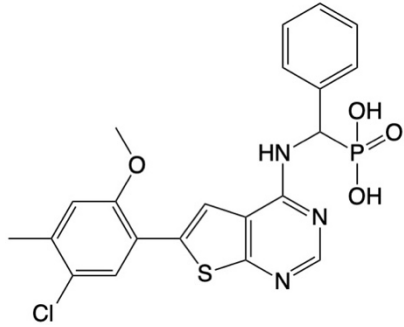
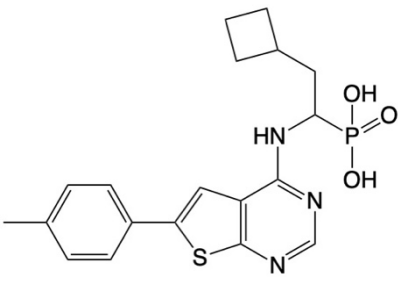
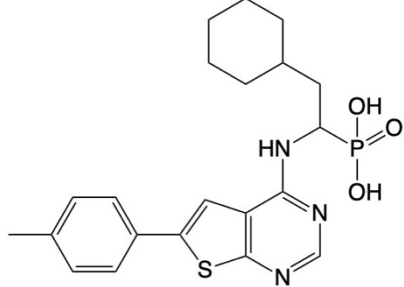
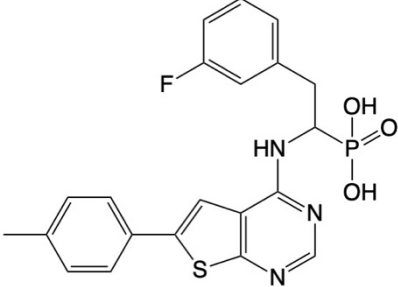
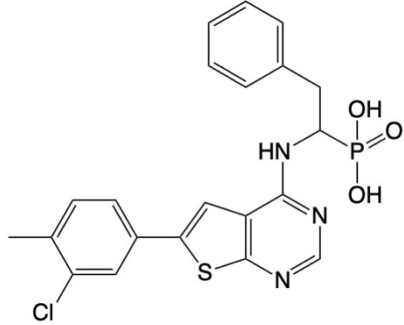
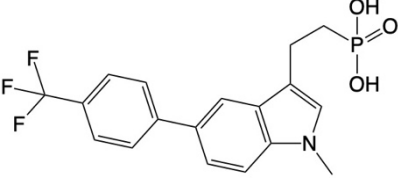
Compound code	Chemical structure	Compound code	Chemical structure
CL-03-51		CL-03-52	
JDS-01-28		JDS-04-71	
JDS-04-72		JDS-05-119	
JDS-07-22		JDS-09-83	

Table 2. Structures of monophosphonate compounds tested in this study.

Compound code	Chemical structure	Compound code	Chemical structure
CL-03-134		CL-06-36	
CL-06-111		CL-08-36	
CL-08-37		CL-08-38	
CL-09-79		YS-09-117	

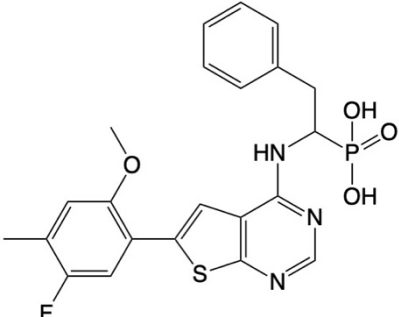
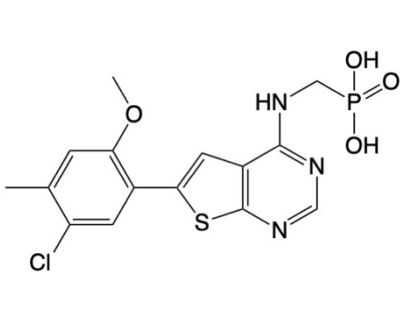
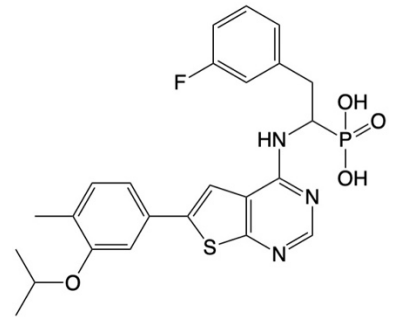
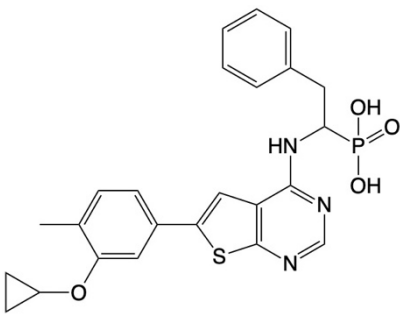
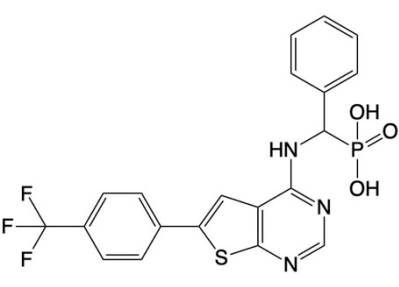
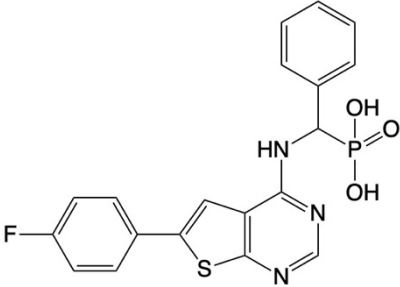
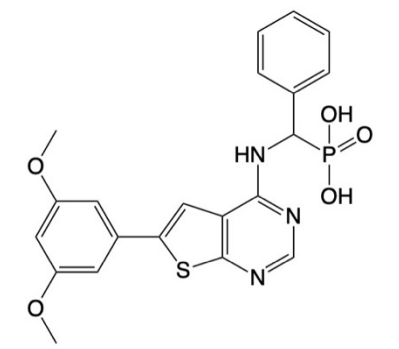
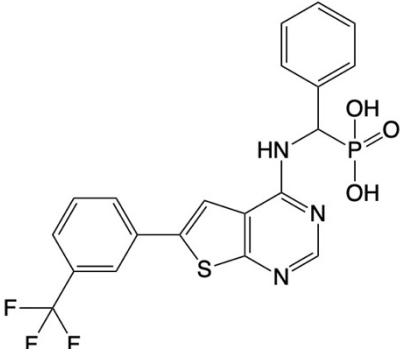
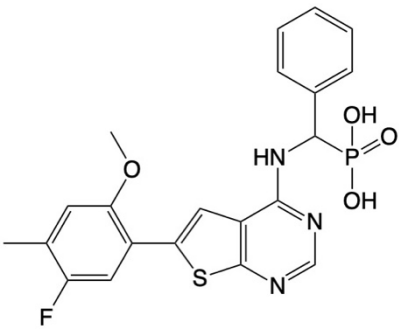
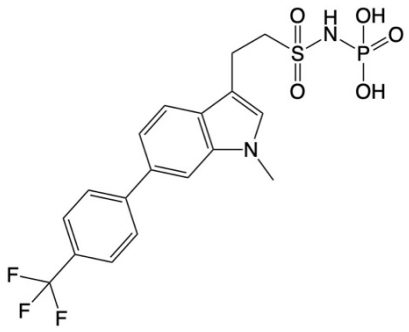
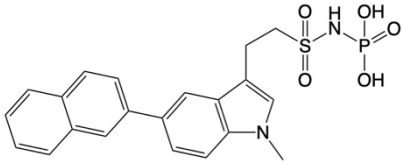
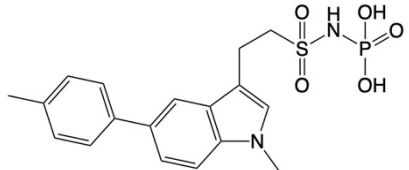
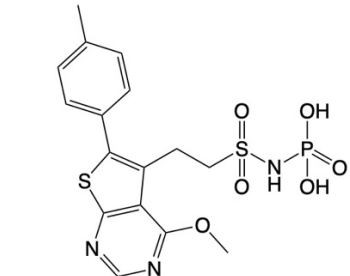
MIT-83		MIT-85	
MIT-149		MIT-150	
WC-01-136		WC-01-137	
WC-01-150		WC-01-151	
WC-02-18			

Table 3. Structures of sulfonylaminophosphonate compounds tested in this study.

Compound code	Chemical structure	Compound code	Chemical structure
YS-09-12		YS-09-51	
YS-09-128		YS-10-35	

Using our standard coupled enzyme assay, I tested the effects of the phosphonate compounds on MK activity at two different concentrations, 1 and 10 μM . MVA and ATP were added at concentrations of 500 and 50 μM , respectively, close to their respective K_m values as determined earlier (i.e., $K_m^{\text{MVA}} = 551 \mu\text{M}$ and $K_m^{\text{ATP}} = 31 \mu\text{M}$). Using substrate concentrations at the K_m values is expected to provide the most reliable screening results when the mode of inhibition is unknown (Yang et al., 2009). Higher substrate concentrations reduce the chance of finding competitive inhibitors, while lower substrate concentrations reduce the chance of finding uncompetitive inhibitors (Acker & Auld, 2014). As a result, I discovered several compounds that potently inhibited the MK-coupled enzyme reaction. In general, bisphosphonates showed limited inhibitory activity (Figure 9c), whereas monophosphonates and sulfonylaminophosphonates exhibited substantial inhibitory effects, with some causing near complete inhibition at 10 μM concentration (Figure 9a and b).

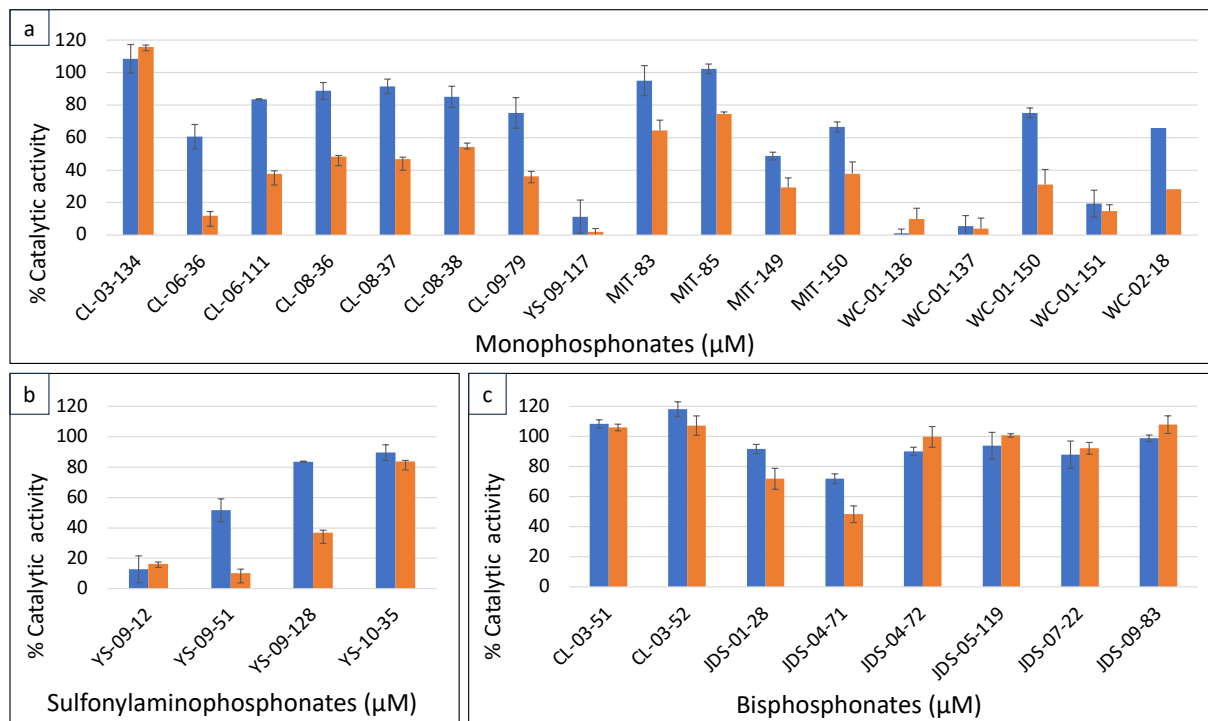


Figure 9. Inhibition of enzyme-coupled MK reaction by phosphonate compounds. Percent inhibition of the reaction rate by monophosphonates (a), sulfonylaminophosphonate (b), and bisphosphonates (c) are displayed separately. The compounds were tested at two concentrations, 1 μM (blue) and 10 μM (orange). Error bars represent the standard deviation of triplicate experiments.

3.4.2 Inhibition of reporter reactions

As I used a coupled enzyme assay to identify the inhibitors described above, it was important to make sure that these compounds decreased the measured reaction rate by inhibiting MK, the target enzyme, rather than the reporter enzymes (i.e., pyruvate kinase and lactate dehydrogenase). To address this concern, I conducted control assays to test whether these compounds could inhibit either of the reporter enzymes. I omitted MK and its substrates (i.e., MVA and ATP) from the reaction buffer and instead, added ADP to drive the coupled reaction. In this reaction, pyruvate kinase converts ADP and phosphoenolpyruvate to ATP and pyruvate, and in turn, lactate dehydrogenase converts pyruvate to lactate by oxidizing NADH to NAD⁺. Only the compounds that had produced greater than 50% inhibition at 10 μM concentration in the previous

screening study were tested, 18 compounds in total, all at a concentration of 10 μM . The results confirmed that these compounds predominantly targeted MK, as they had no significant effects on the coupled enzymes. Most of them showed no inhibitory effects on the MK-omitted, control reaction (grey bars, Figure 10). Six compounds resulted in a reduction in the reaction rate of up to 21%; however, this decrease may fall within the range of experimental uncertainty, as 10 other compounds led to an increase in the reaction rate of up to 32%. I also tested FPP as a control inhibitor, which almost completely inhibited the MK-coupled, standard reaction (98% inhibition) but had no effect on the MK-decoupled, control reaction (Figure 10d).

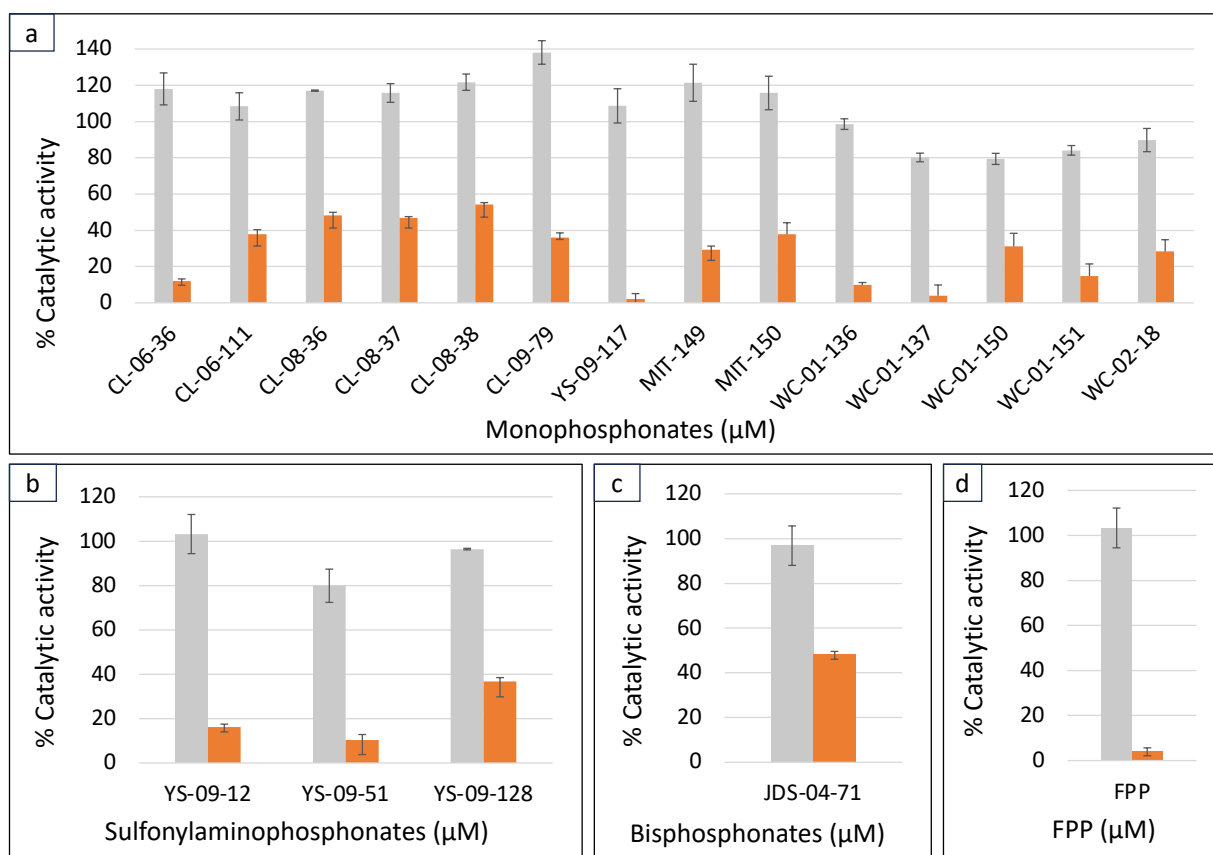


Figure 10. Effects of MK inhibitors on MK-omitted coupled enzyme reaction. Percent catalytic activity in the presence of 10 μM monophosphonates (a), sulfonylaminophosphonates (b), bisphosphonates (c), and FPP (d) is represented by grey bars. Inhibition of the MK-coupled reaction is represented by orange bars for comparison. Error bars represent the standard deviation of duplicate experiments.

3.4.3 IC_{50} determination

To assess the inhibitory potency of the phosphonate compounds more accurately, I determined the IC_{50} values for 13 out of the 18 MK inhibitors tested in the previous study. IC_{50} represents the concentration of an inhibitor required to achieve 50% inhibition of its target enzyme, enabling a quantitative comparison of inhibitor potency. Once again, FPP was used as a control inhibitor, and its IC_{50} was determined to be 12 nM. Among the tested compounds, the most potent inhibitor was the monophosphonate YS-09-117, with an IC_{50} of 8 nM. The next most potent inhibitors were the sulfonylaminophosphonate YS-09-12 and the monophosphonates WC-01-136 and WC-01-137, all with an IC_{50} of ~40 nM. The IC_{50} values for the remaining compounds ranged from 120 nM to 3.3 μ M. The dose-response curves used to determine the IC_{50} values are presented in Figure 11, and the IC_{50} values are provided in Table 4.

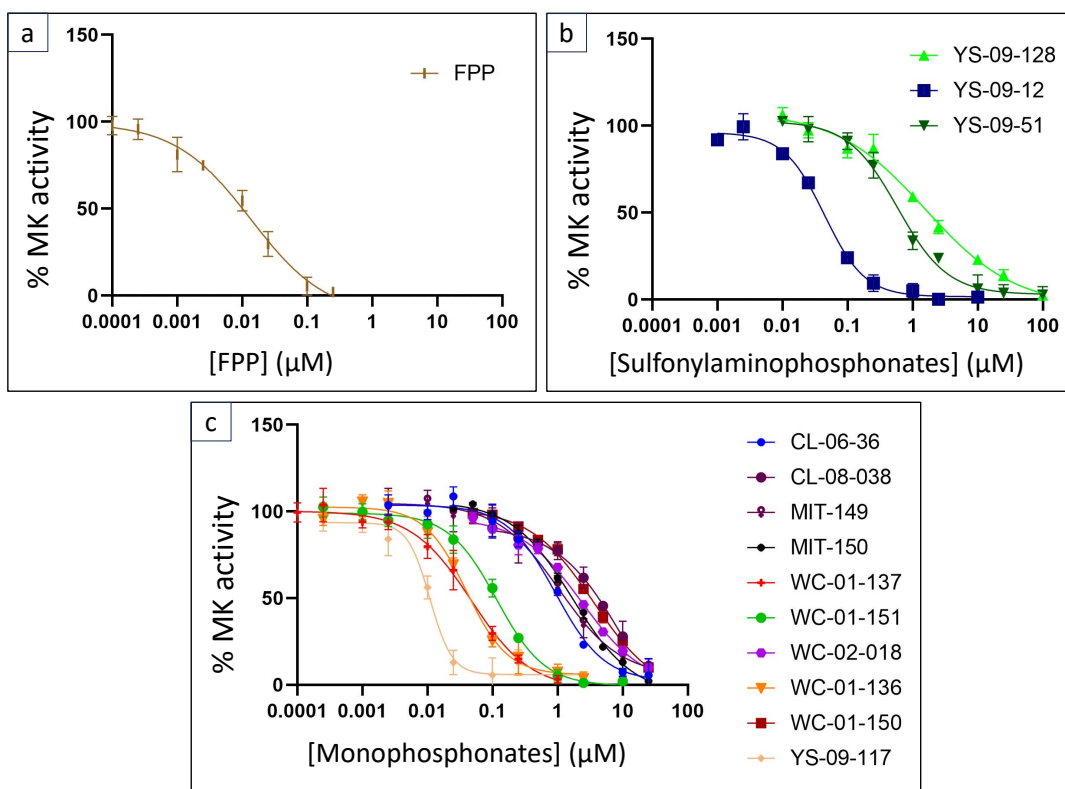


Figure 11. Dose-response curves for IC_{50} determination. a) Monophosphonate inhibitors. b) Sulfonylaminophosphonate inhibitors. c) FPP.

Table 4. IC_{50} of FPP and phosphonate inhibitors for MK inhibition.

Compound	IC_{50} (μ M)
FPP	0.012
CL-06-36	0.965
CL-06-111	1.927
YS-09-12	0.042
YS-09-51	0.583
YS-09-117	0.008
YS-09-128	1.403
MIT-149	1.020
MIT-150	1.639
WC-01-136	0.042
WC-01-137	0.046
WC-01-150	3.255
WC-01-151	0.116
WC-02-018	2.258

3.4.4 Mode of inhibition and K_i determination

Next, I investigated the mechanism by which the phosphonate compounds inhibit MK. Previous studies demonstrated that FPP is a competitive inhibitor with respect to ATP (Fu et al., 2008; Hinson et al., 1997; Potter & Miziorko, 1997). Therefore, if our hypothesis holds true, the phosphonate inhibitors should also exhibit competitive inhibition with respect to ATP. I conducted detailed kinetic analyses, measuring initial rates of the enzyme at a saturating concentration of one substrate and varying concentrations of the other, at four different inhibitor concentrations. Considering the extensive work involved, I only selected the three most potent inhibitors, YS-09-117, YS-09-12, and WC-01-136, for this study. As expected, all three compounds demonstrated a competitive relationship with respect to ATP (left column, Figure 12). The double-reciprocal representations of the rate plots clearly illustrate this inhibition pattern with the lines of different inhibitor concentrations converging on the Y-axis. Conversely, the inhibitors displayed

uncompetitive behaviour with respect to MVA, as evidenced by the series of parallel lines in the double-reciprocal plots (right column, Figure 12). This uncompetitive relationship suggests that the inhibitors bind more tightly to MK in the presence of MVA. In other words, they bind to the enzyme-MVA binary complex with higher affinity than to the unliganded, free enzyme.

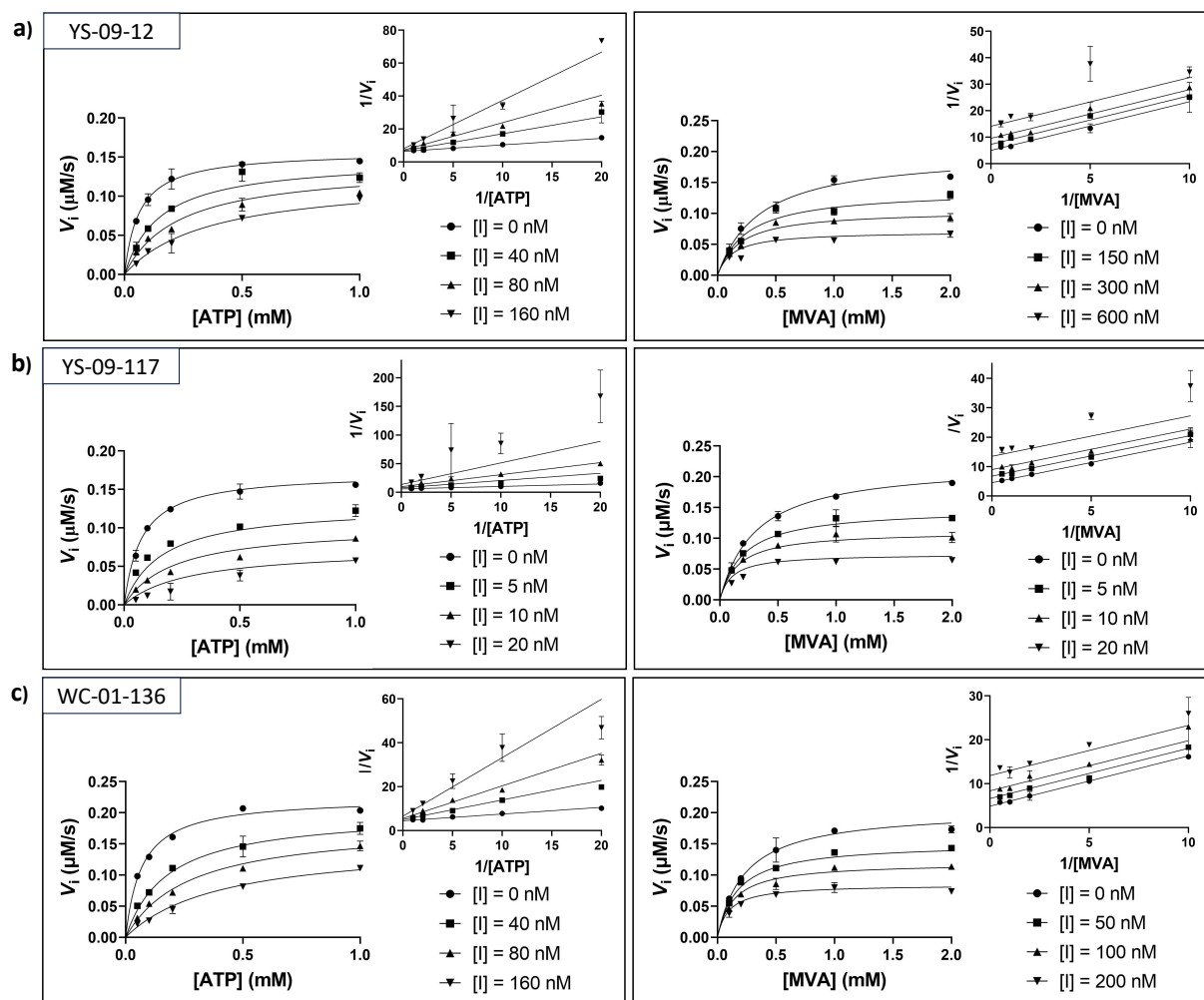


Figure 12. Steady-state kinetic analysis of MK inhibition by phosphonate compounds. a) YS-09-12, b) YS-09-117, and c) WC-01-136. Shown in the insets are the double-reciprocal representations of the initial rate plots. Error bars represent the standard deviation of duplicate experiments.

I could also determine the K_i of the three inhibitors from the rate plots. While IC_{50} values are commonly used as a measure of inhibitor potency, they can be sensitive to measurement conditions and the mode of inhibition of the tested inhibitor. For example, as alluded to above,

using higher substrate concentrations in the inhibition assay may result in higher IC_{50} values for competitive inhibitors. Similarly, lower substrate concentrations can increase the IC_{50} of uncompetitive inhibitors, leading to an underestimation of their potency. This is because lower substrate concentrations result in fewer enzyme-substrate complexes being available for the inhibitor to effectively bind and inhibit. In contrast, the inhibition constant K_i , which describes the binding equilibrium between an inhibitor and its target enzyme, provides a direct measure of their binding affinity and thus offers a more accurate representation of inhibitory potency. The K_i values for YS-09-12, YS-09-117, and WC-01-136 were 25, 2.6, and 21 nM, respectively. In comparison, previously reported K_i values for FPP were 10 nM (Potter & Mizioroko, 1997) and 32 nM (Fu et al., 2008).

3.5 Crystallization studies

The results of the previous kinetic studies indicated that our inhibitors inhibit MK by binding to its ATP binding site. My next objective was to elucidate the details of the enzyme-inhibitor binding through X-ray crystallography. As mentioned in Chapter 1, only one experimental structure of MK is available in the PDB, representing an unliganded state of the enzyme. In addressing this gap, I first attempted to obtain crystals of MK in complex with its substrates. I set up trial plates testing 288 different crystallization conditions using three commercially available screening suites. After several weeks of incubation, I found small crystals in three different crystallization drops (Figure 13). This discovery greatly sparked my optimism that I might be able to solve the elusive structure of an MK-ligand complex.

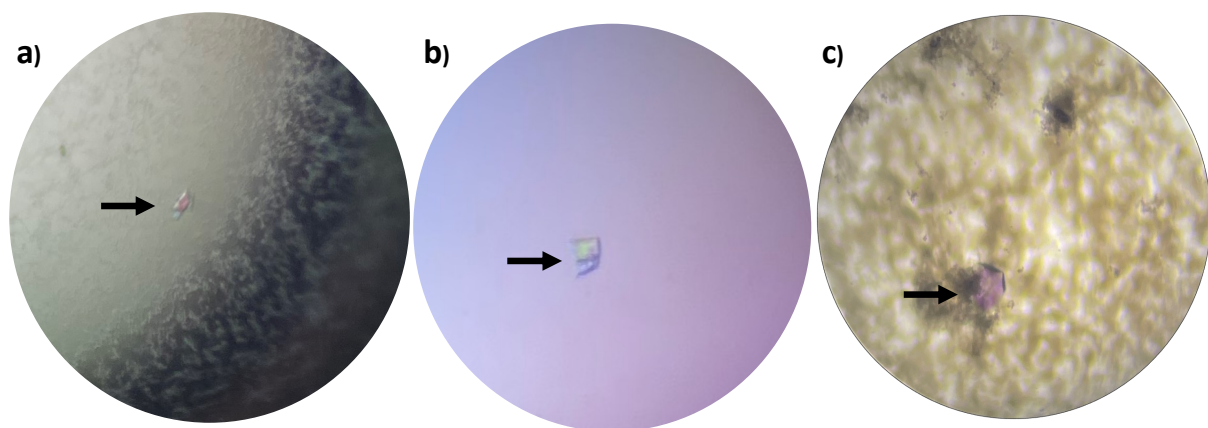


Figure 13. Crystals formed under different crystallization conditions. a) Cluster of three crystals at 4 weeks. Crystallization buffer: 0.1 M Tris (pH 8.5), 8% (w/v) PEG 8000. Crystal size: $30 \times 64 \mu\text{m}$. b) Two crystals fused together at 5 weeks. Crystallization buffer: 0.1 M BICINE (pH 9.0), 2.0 M magnesium chloride. Crystal size: $72 \times 108 \mu\text{m}$. c) Single crystal at 16 weeks. Crystallization buffer: 0.2 M ammonium fluoride, 20% (w/v) PEG 3350. Crystal size: $134 \times 142 \mu\text{m}$.

Subsequently, we analyzed the crystals by X-ray diffraction; Dr. Jian-Bin Lin, the X-ray diffraction facility manager at C-CART (Centre for Chemical Analysis, Research and Training), carried out the diffraction experiments in the presence of Dr. Park. Unfortunately, the collected diffraction images conclusively demonstrated that the crystals from all three conditions were of small molecules, probably salts from the protein or crystallization buffers.

3.6 Computational investigation of MK ligand binding

As I was unable to grow crystals of MK, I turned to molecular docking to explore potential binding interactions between MK and our inhibitors. I used a previously determined structure of rat MK (PDB ID 1KVK), which shares 81.8% sequence identity with human MK, as a reference structure. By superposing this structure onto the unliganded human MK structure (PDB ID 2R3V), I could precisely locate the ATP binding site within the human enzyme. A grid box encompassing the ATP binding site was generated and used as the search space for docking ligands, for which I used AutoDock Vina (Morris et al., 2009). Although it is possible to run docking simulations

without specifying a search grid, doing so is computationally expensive and may increase the likelihood of false positive binding poses.

I first docked ATP as a control ligand (Figure 14a). A comparison with the rat MK structure demonstrated that the docked pose effectively recapitulated the overall position and orientation of the experimentally observed binding pose (Figure 14b). A root-mean-square deviation (RMSD) of less than 1.5 Å is generally considered successful for validating retrospectively docked poses (Hevener et al., 2009); however, such values could not be determined in the absence of any ligand-bound human MK structures. Key interactions between the enzyme and ATP were identified. The main chain amide nitrogen atoms of Gly142 and Gly144, as well as the side chain nitrogen of His197, made close contacts with the triphosphate group of ATP. The side chain hydroxyl of Ser145 and the main chain carbonyl oxygen of Thr104 engaged in interactions with the ring oxygen and the 2' hydroxyl of the ribose group, respectively. The adenine base was deeply buried in a hydrophobic pocket formed by Leu53, Ile56, Ile58, Ala108, Val133, and Tyr149. Subsequently, I carried out docking simulations for all 29 phosphonate compounds examined in this study, as well as FPP. Sample output poses for some of these compounds are presented in Figure 14.

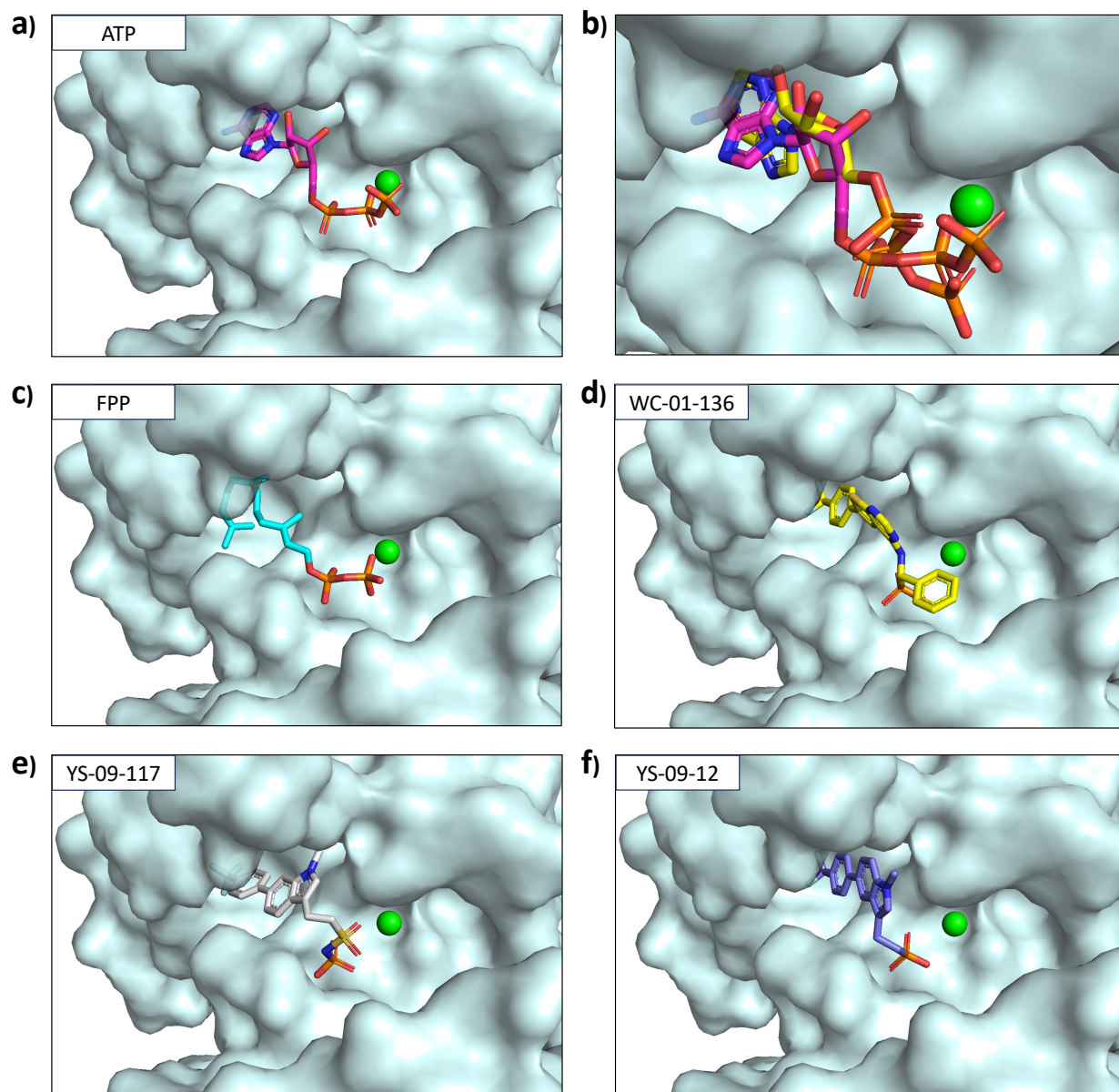


Figure 14. Binding poses of MK ligands as predicted by AutoDock Vina. a) Top scoring docked pose of ATP. b) Superposition of the docked pose (magenta) with the crystallographic binding pose (yellow) observed in a rat MK structure (PDB entry 1KVK). Top scoring docked poses for FPP (c), WC-01-136 (d), YS-09-117 (e), and YS-09-12 (f). Nitrogen atoms are represented in blue, and oxygen atoms in red. The Mg^{2+} ion is shown as a green sphere. The structures were visualized with PyMOL.

AutoDock Vina also estimates the binding energy for the docked ligand using a scoring function that considers factors such as desolvation energy, hydrogen bonding, and torsional strain energy contributing to the ligand-protein interaction (Huey et al., 2007; Trott & Olson, 2010).

Since the potency of competitive inhibitors is directly related to their binding affinity for the target enzyme, inhibitors of MK with lower IC_{50} values should have a greater binding energy. I compared the predicted binding energy to the experimentally determined IC_{50} values, and surprisingly, no statistically significant correlation between the two parameters was present (Figure 15). For example, compounds CL-06-111 and YS-09-117, despite having IC_{50} values that differ by 240-fold, were both predicted to have the same binding energy of -8.8 kcal/mol (Table 5). Further, the bisphosphonate compounds that showed inactivity in inhibiting MK in my earlier experiments were predicted to have a similar binding energy compared to the more potent monophosphonates compounds at around -9 kcal/mol. While the output poses appeared reasonable upon visual inspection, this discrepancy cautions against overinterpretation of my docking results until they are experimentally validated.

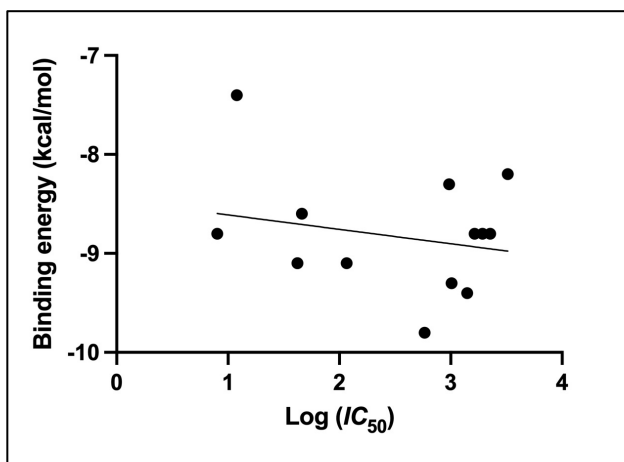


Figure 15. Correlation analysis between measured IC_{50} and predicted binding energy of MK inhibitors. Although a negative correlation with a correlation coefficient of -0.2261 was observed, it was not statistically significant (P value = 0.4369). The analysis was performed with GraphPad Prism.

Table 5. Free energy of binding for MK ligands calculated by AutoDock Vina.

Ligand	Estimated binding energy (kcal/mol)	IC_{50} (μ M)
ATP	-9.2	
FPP	-7.4	0.012
CL-06-36	-8.3	0.965
CL-06-111	-8.8	1.927
YS-09-12	-9.1	0.042
YS-09-51	-9.8	0.583
YS-09-117	-8.8	0.008
YS-09-128	-9.4	1.403
MIT-149	-9.3	1.020
MIT-150	-8.8	1.639
WC-01-136	-9.1	0.042
WC-01-137	-8.6	0.046
WC-01-150	-8.2	3.255
WC-01-151	-9.1	0.116
WC-02-018	-8.8	2.258

Chapter 4. Discussion

4.1 Creation of expression vector

The first critical task in my research project was to obtain an appropriate plasmid construct for the recombinant expression of human MK. This step was of special importance because the success of my entire thesis hinged on having a substantial amount of functionally active enzyme. One key aspect I considered in designing this construct was the inclusion of a His-tag, as it would enable a quick and efficient purification of the recombinantly expressed protein. The six consecutive histidine residues provide a high affinity for immobilized metal affinity columns, making it well suited for Ni-affinity chromatography. Importantly, our lab already had the necessary equipment and expertise for this purification method, as my fellow lab members routinely purified their enzymes of study, such as FPP synthase and GGPP synthase, using the His-tag approach.

However, I also wanted the flexibility to remove the His-tag from my protein when needed. An interesting decision I made was to avoid incorporating the Tobacco Etch Virus (TEV) protease cleavage site, a common choice for removing fusion tags from recombinantly produced proteins. This decision stemmed from the concerns that using TEV protease for tag removal might inadvertently alter the expressed protein, affecting its enzymatic function. To make an informed decision, I used PeptideCutter (Gasteiger et al., 2003), a bioinformatics tool used to predict protease cleavage sites in protein sequences. According to this tool, the human MK sequence contained a potential TEV protease cleavage site, and cleaving at this site would result in a truncated protein. Instead, I chose to include a thrombin cleavage site in the recombinant protein, another commonly used cleavage site for fusion proteins. No potential thrombin cleavage site was detected in the human MK sequence by PeptideCutter.

Another factor I took into consideration was the positioning of the His-tag. It was important to place the tag in a way that the functional domains of the MK protein remained unaltered, to preserve the protein's catalytic function. Fortunately, upon inspecting the available crystal structure, it became evident that neither the N-terminus nor the C-terminus of the protein was part of its active site. Given that the N-terminus was further away from the active site, I decided to position the tag there. After considering all these factors, I decided to clone the MK gene into the pET-15b plasmid. It was confirmed in later experiments that the N-terminal His-tag did not interfere with the enzymatic function of my recombinant protein. Figure 15 provides a visual representation of the expressed human MK sequence, with color-coded segments of interest represented.

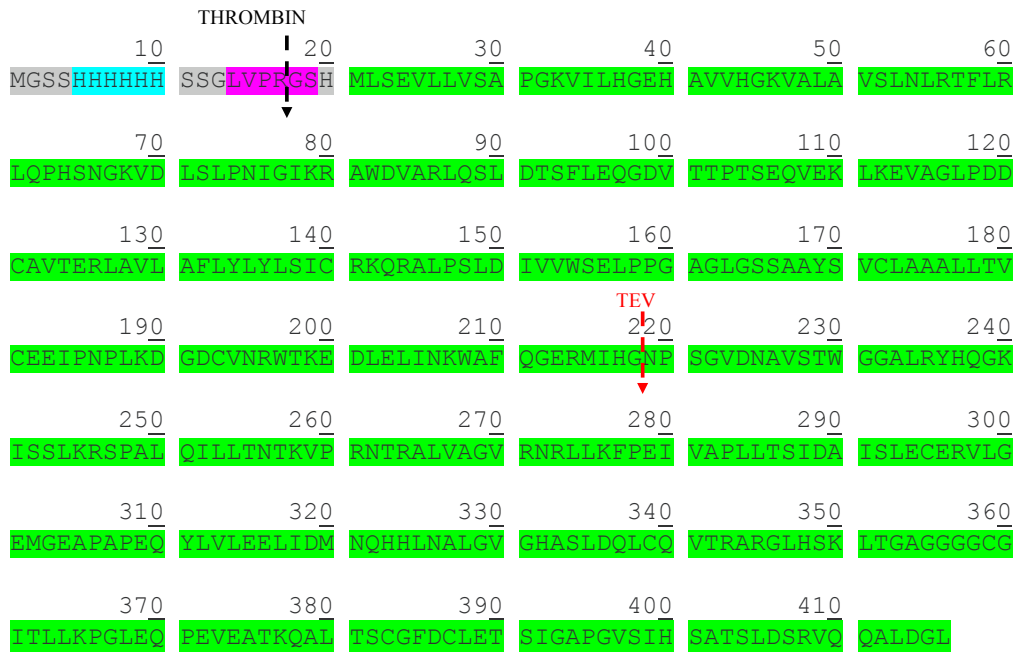


Figure 16. Amino acid sequence annotation of recombinant human MK. The N-terminal His-tag is highlighted in cyan. The thrombin cleavage site is denoted in magenta. The extra amino acids present in the protein as a cloning by-product are represented in grey. The original protein sequence for human MK is represented in green. The potential TEV protease cleavage site predicted by PeptideCutter is indicated by a red arrow. The protein comprises a total of 416 amino acids, with a calculated molecular weight of 44,614.23 Da.

4.2 Protein expression conditions

Through the process of recombinant expression and purification of human MK, I was able to obtain 12 mg of total protein for my subsequent studies. Incidentally, I used up my frozen enzyme stocks just as I was concluding my wet-lab work. While I am relieved that I could complete all my experiments with a single batch of enzyme, thus eliminating the possibility of errors arising from sample variation, it would have been helpful to produce a larger amount of protein that could support follow-up studies spanning 2 to 3 years.

A key consideration during the protein expression process was the choice of incubation temperature. Although I experimented with two temperatures, 37 °C and 26 °C, I would have liked to explore even lower temperatures, such as 18 °C. One notable characteristic of the T7 RNA polymerase-based expression vectors, including pET-15b, is that proteins often precipitate when expressed at 37 °C but remain more soluble when expressed at temperatures in the range of 15 to 25 °C (Vera et al., 2007). This is likely because slower rates of protein production allow newly transcribed proteins sufficient time to fold properly. Unfortunately, I could not explore lower temperature conditions due to the technical limitations of the shaker incubator that was available to me at the time. Since our lab now has the capability for low-temperature incubation, future expression experiments may benefit from adopting an 18 °C overnight expression protocol, potentially leading to an increased protein yield.

4.3 Enzyme-coupled MK assay

Another critical requirement for the success of my research project was a reliable enzyme assay method. To measure the catalytic activity of MK, I adopted a pyruvate kinase-lactate dehydrogenase-coupled assay method (Figure 17). This method is widely used for quantifying the activity of various kinases and was thus deemed suitable for assessing MK activity. It operates on

the following mechanism: ADP generated by the tested kinase is converted to ATP by pyruvate kinase, which concurrently converts phosphoenolpyruvate to pyruvate. Subsequently, pyruvate is converted to lactate by lactate dehydrogenase, which oxidizes NADH to NAD⁺ in the process. Consequently, the reduction in NADH concentration over time corresponds to the rate of ATP hydrolysis. Therefore, the rate of the kinase reaction can be quantified by monitoring the decrease in absorbance at 340 nm.

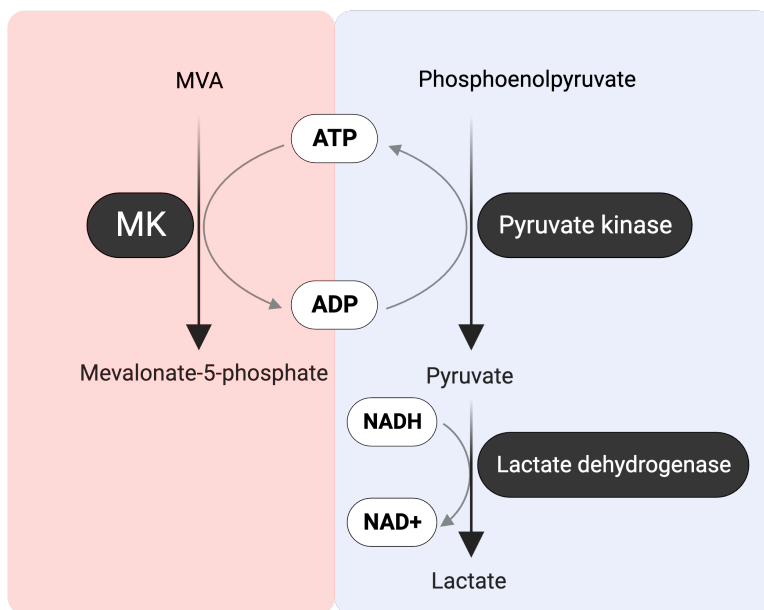


Figure 17. Schematic overview of the pyruvate kinase-lactate dehydrogenase-coupled assay for measuring MK activity. Created with BioRender.com.

As the first and only person in our lab to study MK and use the coupled enzyme assay method, I faced the task of optimizing the assay protocol. The optimization process entailed a comprehensive examination of 16 different assay conditions, which resulted from varying combinations of enzyme and substrate concentrations used in the overall coupled reaction. One of my primary objectives was to ensure an excess of reporter enzymes (i.e., pyruvate kinase and lactate dehydrogenase) and their substrates (i.e., phosphoenolpyruvate and NADH) to prevent any bottlenecking by the reporter enzyme processes. This ensured that the rate of the overall reaction

accurately reflected the rate of MK reaction. Simultaneously, I aimed to avoid excessive use of the reporter enzyme components to minimize unnecessary experimental costs. Maintaining the starting concentration of NADH within a reasonable range was also important because spectrophotometer absorbance measurements become unreliable at values greater than 1. Furthermore, it was essential to strike the right balance between the concentration of MK and the initial concentrations of its substrates (i.e., MVA and ATP) in the reaction. This balance was critical in achieving a sufficient level of MK reaction that could be accurately measured within a reasonable time frame while preventing premature substrate depletion. Other factors I explored and optimized included temperature, incubation periods, absorbance recording intervals, and more. Through these efforts, I was able to establish a robust assay protocol for measuring MK activity. Ultimately, this assay method proved highly effective in identifying potent inhibitors of MK.

4.4 Characterization of human MK inhibitors

To investigate the determinants of potency in phosphonate inhibitors of MK, I conducted a structure-activity relationship analysis. The goal was to identify a relationship between the chemical structures of the inhibitor compounds and their inhibitory effects on MK. This analysis revealed that the key features influencing the inhibitory potency of these compounds primarily resided in two distinct structural components: the head and tail functional groups (inset, Figure 18).

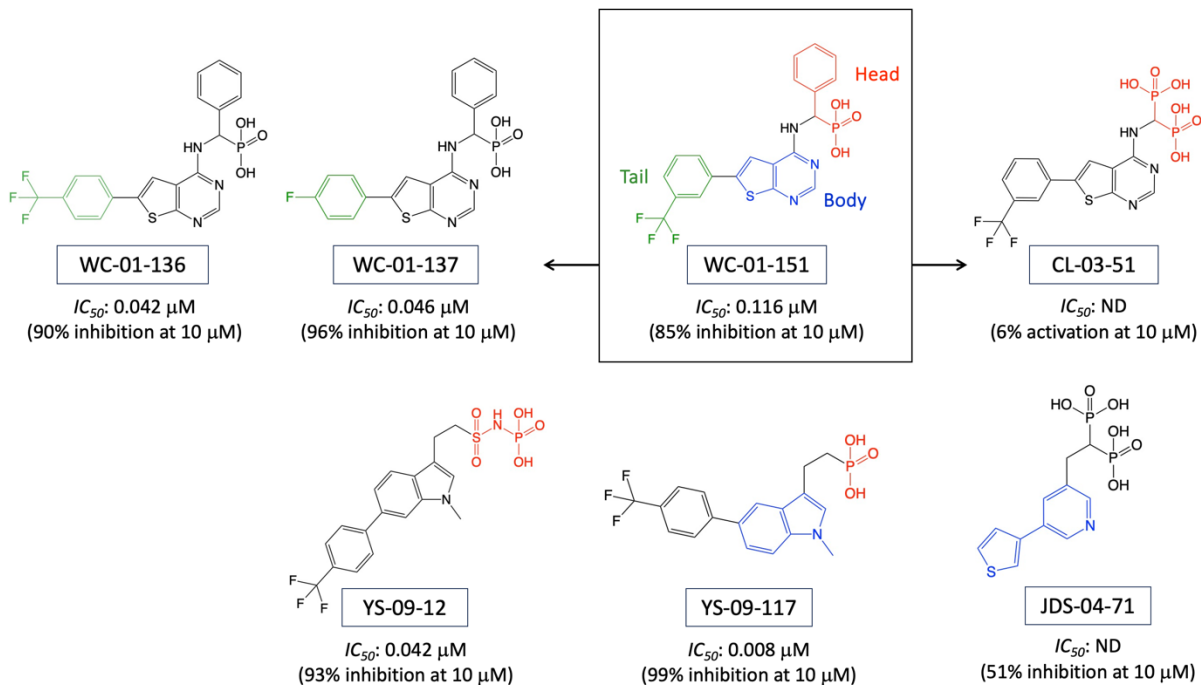


Figure 18. Structural determinants of inhibition potency. Representative inhibitors are displayed with relevant functional groups indicated in different colours. Molecular structures were created with ChemDraw.

The head group emerged as a key determinant of inhibitory potency, with benzylphosphonate (e.g., WC-01-151), sulfonylaminophosphonate (e.g., YS-09-12), and plain monophosphonate (e.g., YS-09-117) moieties showing the greatest inhibitor potency. These functional groups carry a negative charge upon deprotonation under physiological pH and are thus able to mimic the pyrophosphate group of FPP. This mimicry likely allows the inhibitors to compete with ATP for binding to the ATP binding site of MK, similar to how FPP inhibits MK. Surprisingly, bisphosphonate compounds exhibited much lower inhibitory potencies (e.g., WC-01-151 vs. CL-03-51; Figure 18). Bisphosphonates are well-established pyrophosphate analogues and carry a greater negative charge than a monophosphonate group. Therefore, bisphosphonate compounds may be viewed as better mimics of FPP, a pyrophosphate-containing molecule. However, the bisphosphonate group in our compounds is attached to the rest of the compounds

through its geminal carbon atom, unlike the pyrophosphate of FPP, which is connected to the farnesyl group through its α -phosphate in a linear fashion.

The main scaffold, or the ‘body’, of our inhibitor compounds consists of a two-heterocyclic ring system, such as thienopyrimidine (e.g., WC-01-151), methylindole (e.g., YS-09-117), or thiophenylpyridine (e.g., JDS-04-71). There were no significant differences observed between these scaffolds in terms of their contribution to inhibitor potency, especially between thienopyrimidine and methylindole. However, the tail functional group attached to the scaffold significantly impacts inhibitor potency. Typically, the presence of 6-aryl-substitution on the thienopyrimidine scaffold or 5 or 6-aryl-substitution on the methylindole scaffold led to potent inhibitors. Additional functional groups on the terminal aryl ring also contribute to potency, but it is not only the presence of a specific functional group but also its precise location that influences inhibitory activity. For example, incorporating a halogen functional group at the para position of the 6-aryl ring confers higher inhibitory potency than at the meta position (WC-01-136 and WC-01-137 vs. WC-01-151; Figure 18). Conversely, substitution at the ortho position seems to negatively affect the compounds’ inhibitory potency.

4.5 Characterization of inhibitor binding

The kinetic studies and structure-activity relationship analysis have provided some insights into the binding interactions between the phosphonate inhibitors and MK. To gain a deeper understanding of these interactions, I conducted molecular docking and crystallographic studies. Unfortunately, these studies did not produce conclusive results that could be interpreted with a high degree of confidence.

4.5.1 Limitations of molecular docking

My analysis showed no significant correlation between the estimated binding energies and the IC_{50} values obtained experimentally. Several factors may be responsible for the lack of

correlation, including the inherent limitations of molecular docking in capturing dynamic ligand-receptor interactions, the influence of protein flexibility, and the potential for unaccounted factors impacting binding (e.g., the requirement of water molecules to mediate protein-ligand binding). Our results underscore the point that while molecular docking can provide useful insights for some enzyme-inhibitor binding systems, it may not yield reliable results for others. Nevertheless, for our future studies where molecular docking remains a useful tool, several options are worth considering. One approach is to use the flexible docking feature available in AutoDock Vina, which allows specific amino acid side chains to adopt different conformations during the binding of the docked ligand. Additionally, exploring alternative docking programs, such as MOE (Molecular Operating Environment), which is planned for purchase in the near future, may offer new possibilities for improved accuracy and insight in our docking studies.

4.5.2 Strategies for future crystallographic studies

My crystallization trials did not yield crystals of human MK. To address this challenge, we are considering two key modifications to our approach. First, we plan to carry out crystallization trials using MK with the His-tag-removed. It is well accepted that the presence of a His-tag can disrupt protein crystallization processes by introducing increased disorder to the system (Carson et al., 2007)—although it is worth noting that many proteins have successfully crystallized with an intact His-tag, which is why I initially attempted crystallization with it. In our upcoming experiments, we will utilize the thrombin cleavage site to remove the His-tag from the expressed MK protein. This removal should help minimize potential interference in the crystallization process, leading to more consistent and successful crystallization results. Second, we aim to improve the purity of our protein sample for crystallization experiments. It is well established that the success of crystallization is closely linked to protein purity. Greater sample homogeneity is thought to facilitate nucleation and promote crystal growth. Typically, a purity level of greater

than 95% is recommended for crystallization experiments (Kim et al., 2008), whereas the purity of my sample was estimated to be 85%. To achieve higher purity, we can implement an additional step in our purification process, such as an ion-exchange chromatography step. The additional step may effectively remove the remaining protein contaminants, enhancing the homogeneity of our sample. If successful, the crystallographic studies will elucidate the binding interactions between MK and its inhibitors, ultimately contributing to the broader field of drug discovery and protein structure determination.

Chapter 5. Conclusion

In conclusion, this thesis successfully validated my hypothesis that phosphonate analogues of FPP can inhibit MK. Through systemic exploration of compounds originally designed for FPP synthase inhibition, I discovered potent inhibitors of MK with low nanomolar activity. Further characterization revealed their competitive mode of inhibition and identified key structural determinants of their potency. This research forms the foundation for future investigations, including crystallographic studies to enhance our understanding of MK-inhibitor binding interactions. New findings may facilitate the discovery of even more potent inhibitors through structure-based approaches. Furthermore, the inhibitors identified in this study can serve as tools for studying mevalonate pathway regulation in model systems, such as cultured tissues and whole organisms, and for exploring the pharmacological potential of targeting MK. In summary, my findings represent a significant contribution to the field of enzyme biochemistry, offering fresh opportunities for both fundamental research and drug discovery endeavours.

Bibliography

- Acker, M. G., & Auld, D. S. (2014). Considerations for the design and reporting of enzyme assays in high-throughput screening applications. *Perspectives in Science*, 1(1–6), 56–73. <https://doi.org/10.1016/J.PISC.2013.12.001>
- Aparicio, A., Gardner, A., Tu, Y., Savage, A., Berenson, J., & Lichtenstein, A. (1998). In vitro cytoreductive effects on multiple myeloma cells induced by bisphosphonates. *Leukemia* 1998 12:2, 12(2), 220–229. <https://doi.org/10.1038/sj.leu.2400892>
- Berndt, N., Hamilton, A. D., & Sebt, S. M. (2011). Targeting protein prenylation for cancer therapy. *Nature Reviews Cancer* 2011 11:11, 11(11), 775–791. <https://doi.org/10.1038/nrc3151>
- Boissier, S., Magonetto, S., Frappart, L., Cuzin, B., Ebetino, F. H., Delmas, P. D., & Clezardin, P. (1997). Bisphosphonates Inhibit Prostate and Breast Carcinoma Cell Adhesion to Unmineralized and Mineralized Bone Extracellular Matrices. *Cancer Research*. <https://aacrjournals.org/cancerres/article/57/18/3890/503652/Bisphosphonates-Inhibit-Prostate-and-Breast>
- Bork, P., Sander, C., & Valencia, A. (1993). Convergent evolution of similar enzymatic function on different protein folds: The hexokinase, ribokinase, and galactokinase families of sugar kinases. *Protein Science*, 2(1), 31–40. <https://doi.org/10.1002/PRO.5560020104>
- Carson, M., Johnson, D. H., McDonald, H., Brouillette, C., & DeLucas, L. J. (2007). His-tag impact on structure. *Urn:Issn:0907-4449*, 63(3), 295–301. <https://doi.org/10.1107/S0907444906052024>
- Casey, P. (1992). Biochemistry of protein prenylation. *Journal of Lipid Research*, 33(12), 1731–1740. [https://doi.org/10.1016/S0022-2275\(20\)41331-8](https://doi.org/10.1016/S0022-2275(20)41331-8)
- Chabanel, A., Flamm, M., Sung, K. L., Lee, M. M., Schachter, D., & Chien, S. (1983). Influence of cholesterol content on red cell membrane viscoelasticity and fluidity. *Biophysical Journal*, 44(2), 171. [https://doi.org/10.1016/S0006-3495\(83\)84288-X](https://doi.org/10.1016/S0006-3495(83)84288-X)
- Crane, F. L., Hatefi, Y., Lester, R. L., & Widmer, C. (1957). Isolation of a quinone from beef heart mitochondria. *Biochimica et Biophysica Acta*, 25(C), 220–221.

[https://doi.org/10.1016/0006-3002\(57\)90457-2](https://doi.org/10.1016/0006-3002(57)90457-2)

Csizmadia, P., & Csizmadia, P. (1999). *MarvinSketch and MarvinView: Molecule Applets for the World Wide Web*. 1775. <https://doi.org/10.3390/ECSOC-3-01775>

De Schutter, J. W., Shaw, J., Lin, Y. S., & Tsantrizos, Y. S. (2012). Design of potent bisphosphonate inhibitors of the human farnesyl pyrophosphate synthase via targeted interactions with the active site ‘capping’ phenyls. *Bioorganic & Medicinal Chemistry*, 20(18), 5583–5591. <https://doi.org/10.1016/J.BMC.2012.07.019>

De Schutter, J. W., Zaretsky, S., Welbourn, S., Pause, A., & Tsantrizos, Y. S. (2010). Novel bisphosphonate inhibitors of the human farnesyl pyrophosphate synthase. *Bioorganic & Medicinal Chemistry Letters*, 20(19), 5781–5786. <https://doi.org/10.1016/J.BMCL.2010.07.133>

Dorsey, J. K., & Porter, J. W. (1968). The Inhibition of Mevalonic Kinase by Geranyl and Farnesyl Pyrophosphates. *Journal of Biological Chemistry*, 243(18), 4667–4670. [https://doi.org/10.1016/S0021-9258\(18\)93170-4](https://doi.org/10.1016/S0021-9258(18)93170-4)

Drenth, J. P. H., Haagsma, C. J., Van Der Meer, J. W. M., Drenth, J. P. H., van der Meer, J. W. M., Weemaes, C. M. R., Bijlsma, J. W. J., de Graeff-Meeder, E. R., Alcalay, M., Chapelon-Abraic, C., Kahn, M. F., Prieur, A. M., Sibiliala, J., Powell, R. J., Topaloglu, R., Saatfi, U., Scolozzi, R., Lazzarin, P., Monciotti, C. M., ... Espanol, T. (1994). Hyperimmunoglobulinemia D and periodic fever syndrome: the clinical spectrum in a series of 50 patients. *Medicine*, 73(3), 133–144. <https://doi.org/10.1097/00005792-199405000-00002>

Durr, I. F., & Rudney, H. (1960). The Reduction of β -Hydroxy- β -methylglutaryl Coenzyme A to Mevalonic Acid. *Journal of Biological Chemistry*, 235(9), 2572–2578. [https://doi.org/10.1016/S0021-9258\(19\)76915-4](https://doi.org/10.1016/S0021-9258(19)76915-4)

Eberhardt, J., Santos-Martins, D., Tillack, A. F., & Forli, S. (2021). AutoDock Vina 1.2.0: New Docking Methods, Expanded Force Field, and Python Bindings. *Journal of Chemical Information and Modeling*, 61(8), 3891–3898. <https://doi.org/10.1021/acs.jcim.1c00203>

Endo, A. (1992). The discovery and development of HMG-CoA reductase inhibitors. *Journal of*

- Lipid Research*, 33(11), 1569–1582. [https://doi.org/10.1016/S0022-2275\(20\)41379-3](https://doi.org/10.1016/S0022-2275(20)41379-3)
- Farmer, J. A., & Gotto, A. M. (1996). Current and Future Therapeutic Approaches to Hyperlipidemia. *Advances in Pharmacology*, 35(C), 79–114. [https://doi.org/10.1016/S1054-3589\(08\)60275-6](https://doi.org/10.1016/S1054-3589(08)60275-6)
- Faulkner, R., & Jo, Y. (2022). Synthesis, function, and regulation of sterol and nonsterol isoprenoids. *Frontiers in Molecular Biosciences*, 9, 1006822. <https://doi.org/10.3389/fmolb.2022.1006822>
- Favier, L. A., & Schulert, G. S. (2016). Mevalonate kinase deficiency: current perspectives. *The Application of Clinical Genetics*, 9, 101–110. <https://doi.org/10.2147/TACG.S93933>
- Feng, Y., Park, J., Li, S. G., Boutin, R., Viereck, P., Schilling, M. A., Berghuis, A. M., & Tsantrizos, Y. S. (2019). Chirality-Driven Mode of Binding of α -Aminophosphonic Acid-Based Allosteric Inhibitors of the Human Farnesyl Pyrophosphate Synthase (hFPPS). *Journal of Medicinal Chemistry*, 62(21), 9691–9702. <https://doi.org/10.1021/ACS.JMEDCHEM.9B01104>
- Fritz, G., Brachetti, C., Bahlmann, F., Schmidt, M., & Kaina, B. (2002). Rho GTPases in human breast tumours: expression and mutation analyses and correlation with clinical parameters. *British Journal of Cancer* 2002 87:6, 87(6), 635–644. <https://doi.org/10.1038/sj.bjc.6600510>
- Fu, Z., Voynova, N. E., Herdendorf, T. J., Mizioro, H. M., & Kim, J. J. P. (2008). Biochemical and Structural Basis for Feedback Inhibition of Mevalonate Kinase and Isoprenoid Metabolism^{†,‡}. *Biochemistry*, 47(12), 3715–3724. <https://doi.org/10.1021/BI7024386>
- Gasteiger, E., Gattiker, A., Hoogland, C., Ivanyi, I., Appel, R. D., & Bairoch, A. (2003). ExPASy: the proteomics server for in-depth protein knowledge and analysis. *Nucleic Acids Research*, 31(13), 3784–3788. <https://doi.org/10.1093/NAR/GKG563>
- Goldstein, J. L., & Brown, M. S. (1990). Regulation of the mevalonate pathway. *Nature* 1990 343:6257, 343(6257), 425–430. <https://doi.org/10.1038/343425a0>
- Graham, I., Cooney, M. T., Bradley, D., Dudina, A., & Reiner, Z. (2012). Dyslipidemias in the prevention of cardiovascular disease: Risks and causality. *Current Cardiology Reports*,

14(6), 709–720. <https://doi.org/10.1007/s11886-012-0313-7>

- Hevener, K. E., Zhao, W., Ball, D. M., Babaoglu, K., Qi, J., White, S. W., & Lee, R. E. (2009). Validation of molecular docking programs for virtual screening against dihydropteroate synthase. *Journal of Chemical Information and Modeling*, 49(2), 444–460. <https://doi.org/10.1021/ci800293n>
- Hinson, D. D., Chambliss, K. L., Toth, M. J., Tanaka, R. D., & Gibson, K. M. (1997). Post-translational regulation of mevalonate kinase by intermediates of the cholesterol and nonsterol isoprene biosynthetic pathways. *Journal of Lipid Research*, 38(11), 2216–2223. [https://doi.org/10.1016/S0022-2275\(20\)34935-X](https://doi.org/10.1016/S0022-2275(20)34935-X)
- Hoffmann, G., Charpentier, C., Mayatepek, E., Mancini, J., Leichsenring, M., Gibson, K. M., Divry, P., Hrebicek, M., Lehnert, W., Sartor, K., Trefz, F. K., Rating, D., Bremer, H. J., & Nyhan, W. L. (1993). Clinical and Biochemical Phenotype in 11 Patients With Mevalonic Aciduria. *Pediatrics*, 91(5), 915–921. <https://doi.org/10.1542/PEDS.91.5.915>
- Hoffmann, G., Gibson, K. M., Brandt, I. K., Bader, P. I., Wappner, R. S., & Sweetman, L. (2009). Mevalonic Aciduria — An Inborn Error of Cholesterol and Nonsterol Isoprene Biosynthesis. [Http://Dx.Doi.Org/10.1056/NEJM198606193142504](http://Dx.Doi.Org/10.1056/NEJM198606193142504), 314(25), 1610–1614. <https://doi.org/10.1056/NEJM198606193142504>
- Hooff, G. P., Wood, W. G., Müller, W. E., & Eckert, G. P. (2010). Isoprenoids, small GTPases and Alzheimer’s disease. *Biochimica et Biophysica Acta (BBA) - Molecular and Cell Biology of Lipids*, 1801(8), 896–905. <https://doi.org/10.1016/J.BBALIP.2010.03.014>
- Houten, S. M., van Woerden, C. S., Wijburg, F. A., Wanders, R. J. A., & Waterham, H. R. (2003). Carrier frequency of the V377I (1129G>A) MVK mutation, associated with Hyper-IgD and periodic fever syndrome, in the Netherlands. *European Journal of Human Genetics* 2003 11:2, 11(2), 196–200. <https://doi.org/10.1038/sj.ejhg.5200933>
- Huey, R., Morris, G. M., Olson, A. J., & Goodsell, D. S. (2007). A semiempirical free energy force field with charge-based desolvation. *Journal of Computational Chemistry*, 28(6), 1145–1152. <https://doi.org/10.1002/JCC.20634>
- Kang, A., & Lee, T. S. (2016). Secondary Metabolism for Isoprenoid-based Biofuels.

- Biotechnology for Biofuel Production and Optimization*, 35–71.
<https://doi.org/10.1016/B978-0-444-63475-7.00002-9>
- Kavanagh, K. L., Dunford, J. E., Bunkoczi, G., Russell, R. G. G., & Oppermann, U. (2006). The crystal structure of human geranylgeranyl pyrophosphate synthase reveals a novel hexameric arrangement and inhibitory product binding. *Journal of Biological Chemistry*, 281(31), 22004–22012. <https://doi.org/10.1074/jbc.M602603200>
- Khosla, S., & Monroe, D. G. (2018). Regulation of Bone Metabolism by Sex Steroids. *Cold Spring Harbor Perspectives in Medicine*, 8(1), a031211.
<https://doi.org/10.1101/CSHPERSPECT.A031211>
- Kim, Y., Bigelow, L., Borovilos, M., Dementieva, I., Duggan, E., eschenfeldt, W., Hatzos, C., Joachimiak, G., Li, H., Maltseva, N., Mulligan, R., Quartey, P., Sather, A., Stols, L., Volkart, L., Wu, R., Zhou, M., & Joachimiak, A. (2008). High-Throughput Protein Purification for X-Ray Crystallography and NMR. *Advances in Protein Chemistry and Structural Biology*, 75(C), 85–105. [https://doi.org/10.1016/S0065-3233\(07\)75003-9](https://doi.org/10.1016/S0065-3233(07)75003-9)
- Kutner, M. H. (1997). Applied Linear Statistical Models. In *Journal of Quality Technology* (Vol. 29, Issue 2). https://users.stat.ufl.edu/~winner/sta4211/ALSM_5Ed_Kutner.pdf
- Kuzu, O. F., Noory, M. A., & Robertson, G. P. (2016). The role of cholesterol in cancer. *Cancer Research*, 76(8), 2063–2070. <https://doi.org/10.1158/0008-5472.CAN-15-2613>
- Leung, C. Y., Park, J., De Schutter, J. W., Sebag, M., Berghuis, A. M., & Tsantrizos, Y. S. (2013). Thienopyrimidine bisphosphonate (ThPBP) inhibitors of the human farnesyl pyrophosphate synthase: Optimization and characterization of the mode of inhibition. *Journal of Medicinal Chemistry*, 56(20), 7939–7950. <https://doi.org/10.1021/jm400946f>
- Luckman, S. P., Hughes, D. E., Coxon, F. P., Russell, R. G. G., & Rogers, M. J. (1998). Nitrogen-containing bisphosphonates inhibit the mevalonate pathway and prevent post-translational prenylation of GTP-binding proteins, including Ras. *Journal of Bone and Mineral Research : The Official Journal of the American Society for Bone and Mineral Research*, 13(4), 581–589. <https://doi.org/10.1359/JBMR.1998.13.4.581>
- McTaggart, S. J. (2006). Isoprenylated proteins. *Cellular and Molecular Life Sciences*, 63(3),

255–267. <https://doi.org/10.1007/S00018-005-5298-6>

Miziorko, H. M. (2011). Enzymes of the mevalonate pathway of isoprenoid biosynthesis.

Archives of Biochemistry and Biophysics, 505(2), 131–143.

<https://doi.org/10.1016/J.ABB.2010.09.028>

Morgan, G. J., Davies, F. E., Gregory, W. M., Cocks, K., Bell, S. E., Szubert, A. J., Navarro-Coy, N., Drayson, M. T., Owen, R. G., Feyler, S., Ashcroft, A. J., Ross, F., Byrne, J., Roddie, H., Rudin, C., Cook, G., Jackson, G. H., Child, J. A., & Group, on behalf of the N. C. R. I. H. O. C. S. (2010). First-line treatment with zoledronic acid as compared with clodronic acid in multiple myeloma (MRC Myeloma IX): a randomised controlled trial.

Lancet, 376(9757), 744. [https://doi.org/10.1016/S0140-6736\(10\)62051-X](https://doi.org/10.1016/S0140-6736(10)62051-X)

Morris, G. M., Ruth, H., Lindstrom, W., Sanner, M. F., Belew, R. K., Goodsell, D. S., & Olson, A. J. (2009). AutoDock4 and AutoDockTools4: Automated docking with selective receptor flexibility. *Journal of Computational Chemistry*, 30(16), 2785–2791.

<https://doi.org/10.1002/JCC.21256>

Mullen, P. J., Yu, R., Longo, J., Archer, M. C., & Penn, L. Z. (2016). The interplay between cell signalling and the mevalonate pathway in cancer. *Nature Reviews Cancer* 2016 16:11,

16(11), 718–731. <https://doi.org/10.1038/nrc.2016.76>

Park, J., Leung, C. Y., Matralis, A. N., Lacbay, C. M., Tsakos, M., Fernandez De Troconiz, G., Berghuis, A. M., & Tsantrizos, Y. S. (2017). Pharmacophore Mapping of Thienopyrimidine-Based Monophosphonate (ThP-MP) Inhibitors of the Human Farnesyl Pyrophosphate Synthase. *Journal of Medicinal Chemistry*, 60(5), 2119–2134.

<https://doi.org/10.1021/acs.jmedchem.6b01888>

Park, J., Lin, Y. S., De Schutter, J. W., Tsantrizos, Y. S., & Berghuis, A. M. (2012). Ternary complex structures of human farnesyl pyrophosphate synthase bound with a novel inhibitor and secondary ligands provide insights into the molecular details of the enzyme's active site closure. *BMC Structural Biology*, 12(1), 1–12. <https://doi.org/10.1186/1472-6807-12-32>

Park, J., Zielinski, M., Magder, A., Tsantrizos, Y. S., & Berghuis, A. M. (2017). Human farnesyl pyrophosphate synthase is allosterically inhibited by its own product. *Nature Communications*, 8, 1–8. <https://doi.org/10.1038/ncomms14132>

Communications, 8, 1–8. <https://doi.org/10.1038/ncomms14132>

- Pazianas, M., Abrahamsen, B., Eiken, P. A., Eastell, R., Graham, R., & Russell, G. (2012). Reduced colon cancer incidence and mortality in postmenopausal women treated with an oral bisphosphonate - Danish National Register Based Cohort Study. *Osteoporosis International*, 23(11), 2693–2701. <https://doi.org/10.1007/S00198-012-1902-4>
- Popov, V. N., Purvis, A. C., Skulachev, V. P., & Wagner, A. M. (2001). Stress-induced changes in ubiquinone concentration and alternative oxidase in plant mitochondria. *Bioscience Reports*, 21(3), 369–379. <https://doi.org/10.1023/A:1013246501917>
- Potter, D., & Miziorko, H. M. (1997). Identification of Catalytic Residues in Human Mevalonate Kinase. *Journal of Biological Chemistry*, 272(41), 25449–25454. <https://doi.org/10.1074/JBC.272.41.25449>
- Refolo, L. M., Pappolla, M. A., Malester, B., LaFrancois, J., Bryant-Thomas, T., Wang, R., Tint, G. S., Sambamurti, K., & Duff, K. (2000). Hypercholesterolemia Accelerates the Alzheimer's Amyloid Pathology in a Transgenic Mouse Model. *Neurobiology of Disease*, 7(4), 321–331. <https://doi.org/10.1006/NBDI.2000.0304>
- Rogers, Mönkkönen, & Munoz. (2020). Molecular mechanisms of action of bisphosphonates and new insights into their effects outside the skeleton. *Bone*, 139, 115493. <https://doi.org/10.1016/J.BONE.2020.115493>
- Sacchettini, J. C., & Poulter, C. D. (1997). Creating Isoprenoid Diversity. *Science*, 277(5333), 1788–1789. <https://doi.org/10.1126/SCIENCE.277.5333.1788>
- Shipman, C. M., Rogers, M. J., Apperley, J. F., Russell, R. G. G., & Croucher, P. I. (1997). Bisphosphonates induce apoptosis in human myeloma cell lines: a novel anti-tumour activity. *British Journal of Haematology*, 98(3), 665–672. <https://doi.org/10.1046/J.1365-2141.1997.2713086.X>
- Trott, O., & Olson, A. J. (2010). AutoDock Vina: Improving the speed and accuracy of docking with a new scoring function, efficient optimization, and multithreading. *Journal of Computational Chemistry*, 31(2), 455–461. <https://doi.org/10.1002/JCC.21334>
- Valachis, A., Polyzos, N. P., Coleman, R. E., Gnant, M., Eidtmann, H., Brufsky, A. M., Aft, R., Tevaarwerk, A. J., Swenson, K., Lind, P., & Mauri, D. (2013). Adjuvant Therapy With

- Zoledronic Acid in Patients With Breast Cancer: A Systematic Review and Meta-Analysis. *The Oncologist*, 18(4), 353–361. <https://doi.org/10.1634/THEONCOLOGIST.2012-0261>
- Van Der Hilst, J. C. H., Bodar, E. J., Barron, K. S., Frenkel, J., Drenth, J. P. H., Van Der Meer, J. W. M., & Simon, A. (2008). Long-term follow-up, clinical features, and quality of life in a series of 103 patients with hyperimmunoglobulinemia D syndrome. *Medicine*, 87(6), 301–310. <https://doi.org/10.1097/MD.0B013E318190CFB7>
- Van Der Meer, J. W. M., Radl, J., Meyer, C. J. L. M., Vossen, J. M., Van Nieuwkoop, J. A., Lobatto, S., & Van Furth, R. (1984). HYPERIMMUNOGLOBULINAEMIA D AND PERIODIC FEVER: A NEW SYNDROME. *The Lancet*, 323(8386), 1087–1090. [https://doi.org/10.1016/S0140-6736\(84\)92505-4](https://doi.org/10.1016/S0140-6736(84)92505-4)
- Vardy, E. R. L. C., Catto, A. J., & Hooper, N. M. (2005). Proteolytic mechanisms in amyloid- β metabolism: Therapeutic implications for Alzheimer's disease. *Trends in Molecular Medicine*, 11(10), 464–472. <https://doi.org/10.1016/j.molmed.2005.08.004>
- Veldurthy, V., Wei, R., Oz, L., Dhawan, P., Jeon, Y. H., & Christakos, S. (2016). Vitamin D, calcium homeostasis and aging. *Bone Research 2016 4:1*, 4(1), 1–7. <https://doi.org/10.1038/boneres.2016.41>
- Vera, A., González-Montalbán, N., Arís, A., & Villaverde, A. (2007). The conformational quality of insoluble recombinant proteins is enhanced at low growth temperatures. *Biotechnology and Bioengineering*, 96(6), 1101–1106. <https://doi.org/10.1002/BIT.21218>
- Wang, M., & Casey, P. J. (2016). Protein prenylation: unique fats make their mark on biology. *Nature Reviews Molecular Cell Biology 2016 17:2*, 17(2), 110–122. <https://doi.org/10.1038/nrm.2015.11>
- Yang, J., Copeland, R. A., & Lai, Z. (2009). Defining Balanced Conditions for Inhibitor Screening Assays That Target Bisubstrate Enzymes. *SLAS Discovery*, 14(2), 111–120. <https://doi.org/10.1177/1087057108328763>
- Zhang, S. Q., Jiang, T., Li, M., Zhang, X., Ren, Y. Q., Wei, S. C., Sun, L. D., Cheng, H., Li, Y., Yin, X. Y., Hu, Z. M., Wang, Z. Y., Liu, Y., Guo, B. R., Tang, H. Y., Tang, X. F., Ding, Y. T., Wang, J. B., Li, P., ... Zhang, X. J. (2012). Exome sequencing identifies MVK

mutations in disseminated superficial actinic porokeratosis. *Nature Genetics* 2012 44:10, 44(10), 1156–1160. <https://doi.org/10.1038/ng.2409>

Appendix I. Supplemental information

Table S1. The Classics Suite composition.

#	Well	Salt	Buffer	Precipitant	100 ml Refill SKU
1	A1	0.01 M Cobalt chloride	0.1 M Sodium acetate pH 4.6	1.0 M 1,6-Hexanediol	134001-1
2	A2		0.1 M tri-Sodium citrate pH 5.6	2.5 M 1,6-Hexanediol	134001-2
3	A3	0.2 M Magnesium chloride	0.1 M Tris pH 8.5	3.4 M 1,6-Hexanediol	134001-3
4	A4	2.0M Ammonium sulfate		5% (v/v) Isopropanol	134001-4
5	A5		0.1 M HEPES sodium salt pH 7.5	10% (v/v) Isopropanol; 20% (w/v) PEG 4000	134001-5
6	A6	0.2 M Calcium chloride	0.1 M Sodium acetate pH 4.6	20% (v/v) Isopropanol	134001-6
7	A7		0.1 M tri-Sodium citrate pH 5.6	20% (v/v) Isopropanol; 20% (w/v) PEG 4000	134001-7
8	A8	0.2 M tri-Sodium citrate	0.1 M HEPES sodium salt pH 7.5	20% (v/v) Isopropanol	134001-8
9	A9	0.2 M tri-Sodium citrate	0.1 M Sodium cacodylate pH 6.5	30% (v/v) Isopropanol	134001-9
10	A10	0.2 M Magnesium chloride	0.1 M HEPES sodium salt pH 7.5	30% (v/v) Isopropanol	134001-10
11	A11	0.2 M Ammonium acetate	0.1 M Tris-HCl pH 8.5	30% (v/v) Isopropanol	134001-11
12	A12	1.5 M Sodium chloride		10% (v/v) Ethanol	134001-12
13	B1		0.1 M Tris pH 8.5	20% (v/v) Ethanol	134001-13
14	B2			25% (v/v) Ethylene glycol	134001-14
15	B3	0.02 M Calcium chloride	0.1 M Sodium acetate pH 4.6	30% (v/v) MPD	134001-15
16	B4	0.2 M Sodium chloride	0.1 M Sodium acetate pH 4.6	30% (v/v) MPD	134001-16
17	B5	0.2 M Ammonium acetate	0.1 M tri-Sodium citrate pH 5.6	30% (v/v) MPD	134001-17
18	B6	0.2 M Magnesium acetate	0.1 M Sodium cacodylate pH 6.5	30% (v/v) MPD	134001-18
19	B7	0.2 M tri-Sodium citrate	0.1 M HEPES sodium salt pH 7.5	30% (v/v) MPD	134001-19
20	B8	0.5 M Ammonium sulfate	0.1 M HEPES pH 7.5	30% (v/v) MPD	134001-20
21	B9	0.2 M Ammonium phosphate	0.1 M Tris pH 8.5	50% (v/v) MPD	134001-21
22	B10		0.1 M HEPES pH 7.5	70% (v/v) MPD	134001-22
23	B11		0.1 M Tris pH 8.5	25% (v/v) tert-Butanol	134001-23
24	B12		0.1 M tri-Sodium citrate pH 5.6	35% (v/v) tert-Butanol	134001-24
25	C1			0.4 M Ammonium phosphate	134001-25
26	C2		0.1 M tri-Sodium citrate pH 5.6	1.0 M Ammonium phosphate	134001-26
27	C3		0.1 M Tris-HCl pH 8.5	2.0 M Ammonium phosphate	134001-27
28	C4		0.1 M HEPES pH 7.5	2.0 M Ammonium formate	134001-28
29	C5		0.1 M Sodium acetate pH 4.6	2.0 M Ammonium sulfate	134001-29
30	C6		0.1 M Tris-HCl pH 8.5	2.0 M Ammonium sulfate	134001-30
31	C7			2.0 M Ammonium sulfate	134001-31
32	C8	0.1 M Sodium chloride	0.1 M HEPES pH 7.5	1.6 M Ammonium sulfate	134001-32
33	C9	0.01 M Cobalt chloride	0.1 M MES pH 6.5	1.8 M Ammonium sulfate	134001-33
34	C10	0.2 M K/Na tartrate	0.1 M tri-Sodium citrate pH 5.6	2.0 M Ammonium sulfate	134001-34
35	C11			1.0 M Imidazole pH 7.0	134001-35
36	C12			0.4 M K/Na tartrate	134001-36
37	D1		0.1 M HEPES sodium salt pH 7.5	0.8 M K/Na tartrate	134001-37
38	D2		0.1 M Imidazole pH 6.5	1.0 M Sodium acetate	134001-38
39	D3	0.05 M Cadmium sulfate	0.1 M HEPES pH 7.5	1.0 M Sodium acetate	134001-39
40	D4		0.1 M Sodium cacodylate pH 6.5	1.4 M Sodium acetate	134001-40
41	D5		0.1 M Sodium acetate pH 4.6	2.0 M Sodium chloride	134001-41
42	D6	0.1 M Sodium phosphate; 0.1 M Potassium phosphate	0.1 M MES pH 6.5	2.0 M Sodium chloride	134001-42
43	D7		0.1 M HEPES pH 7.5	4.3 M Sodium chloride	134001-43
44	D8		0.1 M HEPES sodium salt pH 7.5	1.4 M tri-Sodium citrate	134001-44
45	D9			1.6 M tri-Sodium citrate pH 6.5	134001-45
46	D10		0.1 M HEPES sodium salt pH 7.5	0.8 M Sodium phosphate; 0.8 M Potassium phosphate	134001-46
47	D11		0.1 M Sodium acetate pH 4.6	2.0 M Sodium formate	134001-47
48	D12			4.0 M Sodium formate	134001-48
49	E1		0.1 M Bicine pH 9.0	2% (v/v) Dioxane; 10% (w/v) PEG 20000	134001-49

#	Well	Salt	Buffer	Precipitant	100 ml Refill SKU
50	E2	1.6 M Ammonium sulfate	0.1 M MES pH 6.5	10% (v/v) Dioxane	134001-50
51	E3			35% (v/v) Dioxane	134001-51
52	E4	0.5 M Sodium chloride	0.1 M tri-Sodium citrate pH 5.6	2% (v/v) Ethylene imine polymer	134001-52
53	E5	1.5 M Ammonium sulfate	0.1 M Tris pH 8.5	12% (v/v) Glycerol	134001-53
54	E6	0.5 M Sodium chloride; 0.01 M Magnesium chloride		0.01 M CTAB	134001-54
55	E7	0.01 M Ferric chloride	0.1 M tri-Sodium citrate pH 5.6	10 % (v/v) Jeffamine M-600	134001-55
56	E8		0.1 M HEPES pH 7.5	20 % (v/v) Jeffamine M-600	134001-56
57	E9	0.5 M Ammonium sulfate	0.1 M tri-Sodium citrate pH 5.6	1.0 M Lithium sulfate	134001-57
58	E10	0.01 M Nickel chloride	0.1 M TRIS pH 8.5	1.0 M Lithium sulfate	134001-58
59	E11		0.1 M HEPES sodium salt pH 7.5	1.5 M Lithium sulfate	134001-59
60	E12		0.1 M BICINE pH 9.0	2.0 M Magnesium chloride	134001-60
61	F1			0.2 M Magnesium formate	134001-61
62	F2		0.1 M MES pH 6.5	1.6 M Magnesium sulfate	134001-62
63	F3		0.1 M TRIS.HCl pH 8.5	8 % (w/v) PEG 8000	134001-63
64	F4		0.1 M HEPES pH 7.5	10 % (w/v) PEG 8000	134001-64
65	F5	0.5 M Lithium sulfate		15 % (w/v) PEG 8000	134001-65
66	F6	0.2 M Zinc acetate	0.1 M Sodium cacodylate pH 6.5	18 % (w/v) PEG 8000	134001-66
67	F7	0.2 M Calcium acetate	0.1 M Sodium cacodylate pH 6.5	18 % (w/v) PEG 8000	134001-67
68	F8	0.2 M Magnesium acetate	0.1 M Sodium cacodylate pH 6.5	20 % (w/v) PEG 8000	134001-68
69	F9	0.05 M Potassium phosphate		20 % (w/v) PEG 8000	134001-69
70	F10	0.2 M Ammonium sulfate	0.1 M Sodium cacodylate pH 6.5	30 % (w/v) PEG 8000	134001-70
71	F11	0.2 M Sodium acetate	0.1 M Sodium cacodylate pH 6.5	30 % (w/v) PEG 8000	134001-71
72	F12	0.2 M Ammonium sulfate		30 % (w/v) PEG 8000	134001-72
73	G1	2.0 M Ammonium sulfate	0.1 M HEPES sodium salt pH 7.5	2 % (v/v) PEG 400	134001-73
74	G2	0.2 M Calcium chloride	0.1 M HEPES sodium salt pH 7.5	28 % (v/v) PEG 400	134001-74
75	G3	0.1 M Cadmium chloride	0.1 M Sodium acetate pH 4.6	30 % (v/v) PEG 400	134001-75
76	G4	0.2 M Magnesium chloride	0.1 M HEPES sodium salt pH 7.5	30 % (v/v) PEG 400	134001-76
77	G5	0.2 M tri-Sodium citrate	0.1 M TRIS.HCl pH 8.5	30 % (v/v) PEG 400	134001-77
78	G6	0.1 M Sodium chloride	0.1 M BICINE pH 9.0	20 % (w/v) PEG 550 MME	134001-78
79	G7	0.01 M Zinc sulfate	0.1 M MES pH 6.5	25 % (w/v) PEG 550 MME	134001-79
80	G8			10 % (w/v) PEG 1000; 10 % (w/v) PEG 8000	134001-80
81	G9			30 % (w/v) PEG 1500	134001-81
82	G10	0.01 M Nickel chloride	0.1 M TRIS pH 8.5	20 % (w/v) PEG 2000 MME	134001-82
83	G11	0.2 M Ammonium sulfate	0.1 M Sodium acetate pH 4.6	30 % (w/v) PEG 2000 MME	134001-83
84	G12		0.1 M Sodium acetate pH 4.6	8 % (w/v) PEG 4000	134001-84
85	H1	0.2 M Ammonium sulfate	0.1 M Sodium acetate pH 4.6	25 % (w/v) PEG 4000	134001-85
86	H2	0.2 M Ammonium acetate	0.1 M Sodium acetate pH 4.6	30 % (w/v) PEG 4000	134001-86
87	H3	0.2 M Ammonium acetate	0.1 M tri-Sodium citrate pH 5.6	30 % (w/v) PEG 4000	134001-87
88	H4	0.2 M Magnesium chloride	0.1 M TRIS.HCl pH 8.5	30 % (w/v) PEG 4000	134001-88
89	H5	0.2 M Lithium sulfate	0.1 M TRIS.HCl pH 8.5	30 % (w/v) PEG 4000	134001-89
90	H6	0.2 M Sodium acetate	0.1 M TRIS.HCl pH 8.5	30 % (w/v) PEG 4000	134001-90
91	H7	0.2 M Ammonium sulfate		30 % (w/v) PEG 4000	134001-91
92	H8	0.2 M Ammonium sulfate	0.1 M MES pH 6.5	30 % (w/v) PEG 5000 MME	134001-92
93	H9		0.1 M HEPES pH 7.5	10 % (w/v) PEG 6000; 5 % (v/v) MPD	134001-93
94	H10	2.0 M Sodium chloride		10 % (w/v) PEG 6000	134001-94
95	H11		0.1 M HEPES pH 7.5	20 % (w/v) PEG 10000; 8 % (v/v) Ethylene glycol	134001-95
96	H12		0.1 M MES pH 6.5	12 % (w/v) PEG 20000	134001-96

Table S2. The PEGs Suite composition.

#	Well	Salt	Buffer	Precipitant	100 ml Refill SKU
1	A1		0.1 M Sodium acetate pH 4.6	40% (v/v) PEG 200	134301-01
2	A2		0.1 M Sodium acetate pH 4.6	30% (v/v) PEG 300	134301-02
3	A3		0.1 M Sodium acetate pH 4.6	30% (v/v) PEG 400	134301-03
4	A4		0.1 M Sodium acetate pH 4.6	25% (v/v) PEG 550 MME	134301-04
5	A5		0.1 M Sodium acetate pH 4.6	25% (w/v) PEG 1000	134301-05
6	A6		0.1 M Sodium acetate pH 4.6	25% (w/v) PEG 2000 MME	134301-06
7	A7		0.1 M MES pH 6.5	40% (v/v) PEG 200	134301-07
8	A8		0.1 M MES pH 6.5	30% (v/v) PEG 300	134301-08
9	A9		0.1 M MES pH 6.5	30% (v/v) PEG 400	134301-09
10	A10		0.1 M MES pH 6.5	25% (v/v) PEG 550 MME	134301-10
11	A11		0.1 M MES pH 6.5	25% (w/v) PEG 1000	134301-11
12	A12		0.1 M MES pH 6.5	25% (w/v) PEG 2000 MME	134301-12
13	B1		0.1 M Sodium HEPES pH 7.5	40% (v/v) PEG 200	134301-13
14	B2		0.1 M Sodium HEPES pH 7.5	30% (v/v) PEG 300	134301-14
15	B3		0.1 M Sodium HEPES pH 7.5	30% (v/v) PEG 400	134301-15
16	B4		0.1 M Sodium HEPES pH 7.5	25% (v/v) PEG 550 MME	134301-16
17	B5		0.1 M Sodium HEPES pH 7.5	25% (w/v) PEG 1000	134301-17
18	B6		0.1 M Sodium HEPES pH 7.5	25% (w/v) PEG 2000 MME	134301-18
19	B7		0.1 M TRIS.HCl pH 8.5	40% (v/v) PEG 200	134301-19
20	B8		0.1 M TRIS.HCl pH 8.5	30% (v/v) PEG 300	134301-20
21	B9		0.1 M TRIS.HCl pH 8.5	30% (v/v) PEG 400	134301-21
22	B10		0.1 M TRIS.HCl pH 8.5	25% (v/v) PEG 550 MME	134301-22
23	B11		0.1 M TRIS.HCl pH 8.5	25% (w/v) PEG 1000	134301-23
24	B12		0.1 M TRIS.HCl pH 8.5	25% (w/v) PEG 2000 MME	134301-24
25	C1		0.1 M Sodium acetate pH 4.6	25% (w/v) PEG 3000	134301-25
26	C2		0.1 M Sodium acetate pH 4.6	25% (w/v) PEG 4000	134301-26
27	C3		0.1 M Sodium acetate pH 4.6	25% (w/v) PEG 6000	134301-27
28	C4		0.1 M Sodium acetate pH 4.6	25% (w/v) PEG 8000	134301-28
29	C5		0.1 M Sodium acetate pH 4.6	20% (w/v) PEG 10000	134301-29
30	C6		0.1 M Sodium acetate pH 4.6	15% (w/v) PEG 20000	134301-30
31	C7		0.1 M MES pH 6.5	25% (w/v) PEG 3000	134301-31
32	C8		0.1 M MES pH 6.5	25% (w/v) PEG 4000	134301-32
33	C9		0.1 M MES pH 6.5	25% (w/v) PEG 6000	134301-33
34	C10		0.1 M MES pH 6.5	25% (w/v) PEG 8000	134301-34
35	C11		0.1 M MES pH 6.5	20% (w/v) PEG 10000	134301-35
36	C12		0.1 M MES pH 6.5	15% (w/v) PEG 20000	134301-36
37	D1		0.1 M Sodium HEPES pH 7.5	25% (w/v) PEG 3000	134301-37
38	D2		0.1 M Sodium HEPES pH 7.5	25% (w/v) PEG 4000	134301-38
39	D3		0.1 M Sodium HEPES pH 7.5	25% (w/v) PEG 6000	134301-39
40	D4		0.1 M Sodium HEPES pH 7.5	25% (w/v) PEG 8000	134301-40
41	D5		0.1 M Sodium HEPES pH 7.5	20% (w/v) PEG 10000	134301-41
42	D6		0.1 M Sodium HEPES pH 7.5	15% (w/v) PEG 20000	134301-42
43	D7		0.1 M TRIS.HCl pH 8.5	25% (w/v) PEG 3000	134301-43
44	D8		0.1 M TRIS.HCl pH 8.5	25% (w/v) PEG 4000	134301-44
45	D9		0.1 M TRIS.HCl pH 8.5	25% (w/v) PEG 6000	134301-45
46	D10		0.1 M TRIS.HCl pH 8.5	25% (w/v) PEG 8000	134301-46
47	D11		0.1 M TRIS.HCl pH 8.5	20% (w/v) PEG 10000	134301-47
48	D12		0.1 M TRIS.HCl pH 8.5	15% (w/v) PEG 20000	134301-48

#	Well	Salt	Buffer	Precipitant	100 ml Refill SKU
49	E1	0.2 M Sodium fluoride		20% (w/v) PEG 3350	134301-49
50	E2	0.2 M Potassium fluoride		20% (w/v) PEG 3350	134301-50
51	E3	0.2 M Ammonium fluoride		20% (w/v) PEG 3350	134301-51
52	E4	0.2 M Lithium chloride		20% (w/v) PEG 3350	134301-52
53	E5	0.2 M Magnesium chloride		20% (w/v) PEG 3350	134301-53
54	E6	0.2 M Sodium chloride		20% (w/v) PEG 3350	134301-54
55	E7	0.2 M Calcium chloride		20% (w/v) PEG 3350	134301-55
56	E8	0.2 M Potassium chloride		20% (w/v) PEG 3350	134301-56
57	E9	0.2 M Ammonium chloride		20% (w/v) PEG 3350	134301-57
58	E10	0.2 M Sodium iodide		20% (w/v) PEG 3350	134301-58
59	E11	0.2 M Potassium iodide		20% (w/v) PEG 3350	134301-59
60	E12	0.2 M Ammonium iodide		20% (w/v) PEG 3350	134301-60
61	F1	0.2 M Sodium thiocyanate		20% (w/v) PEG 3350	134301-61
62	F2	0.2 M Potassium thiocyanate		20% (w/v) PEG 3350	134301-62
63	F3	0.2 M Lithium nitrate		20% (w/v) PEG 3350	134301-63
64	F4	0.2 M Magnesium nitrate		20% (w/v) PEG 3350	134301-64
65	F5	0.2 M Sodium nitrate		20% (w/v) PEG 3350	134301-65
66	F6	0.2 M Potassium nitrate		20% (w/v) PEG 3350	134301-66
67	F7	0.2 M Ammonium nitrate		20% (w/v) PEG 3350	134301-67
68	F8	0.2 M Magnesium formate		20% (w/v) PEG 3350	134301-68
69	F9	0.2 M Sodium formate		20% (w/v) PEG 3350	134301-69
70	F10	0.2 M Potassium formate		20% (w/v) PEG 3350	134301-70
71	F11	0.2 M Ammonium formate		20% (w/v) PEG 3350	134301-71
72	F12	0.2 M Lithium acetate		20% (w/v) PEG 3350	134301-72
73	G1	0.2 M Magnesium acetate		20% (w/v) PEG 3350	134301-73
74	G2	0.2 M Zinc acetate		20% (w/v) PEG 3350	134301-74
75	G3	0.2 M Sodium acetate		20% (w/v) PEG 3350	134301-75
76	G4	0.2 M Calcium acetate		20% (w/v) PEG 3350	134301-76
77	G5	0.2 M Potassium acetate		20% (w/v) PEG 3350	134301-77
78	G6	0.2 M Ammonium acetate		20% (w/v) PEG 3350	134301-78
79	G7	0.2 M Lithium sulfate		20% (w/v) PEG 3350	134301-79
80	G8	0.2 M Magnesium sulfate		20% (w/v) PEG 3350	134301-80
81	G9	0.2 M Sodium sulfate		20% (w/v) PEG 3350	134301-81
82	G10	0.2 M Potassium sulfate		20% (w/v) PEG 3350	134301-82
83	G11	0.2 M Ammonium sulfate		20% (w/v) PEG 3350	134301-83
84	G12	0.2 M di-Sodium tartrate		20% (w/v) PEG 3350	134301-84
85	H1	0.2 M K/Na tartrate		20% (w/v) PEG 3350	134301-85
86	H2	0.2 M di-Ammonium tartrate		20% (w/v) PEG 3350	134301-86
87	H3	0.2 M Sodium phosphate		20% (w/v) PEG 3350	134301-87
88	H4	0.2 M di-Sodium phosphate		20% (w/v) PEG 3350	134301-88
89	H5	0.2 M Potassium phosphate		20% (w/v) PEG 3350	134301-89
90	H6	0.2 M di-Potassium phosphate		20% (w/v) PEG 3350	134301-90
91	H7	0.2 M Ammonium phosphate		20% (w/v) PEG 3350	134301-91
92	H8	0.2 M di-Ammonium phosphate		20% (w/v) PEG 3350	134301-92
93	H9	0.2 M tri-Lithium citrate		20% (w/v) PEG 3350	134301-93
94	H10	0.2 M tri-Sodium citrate		20% (w/v) PEG 3350	134301-94
95	H11	0.2 M tri-Potassium citrate		20% (w/v) PEG 3350	134301-95
96	H12	0.18 M tri-Ammonium citrate		20% (w/v) PEG 3350	134301-96

Table S3. The AmSO4 Suite composition.

#	Well	Salt	Buffer	Precipitant	100 ml Refill SKU
1	A1			2.2 M Ammonium sulfate	134401-1
2	A2	0.2 M Ammonium acetate		2.2 M Ammonium sulfate	134401-2
3	A3	0.2 M Ammonium chloride		2.2 M Ammonium sulfate	134401-3
4	A4	0.2 M Ammonium phosphate		2.2 M Ammonium sulfate	134401-4
5	A5	0.2 M Ammonium fluoride		2.2 M Ammonium sulfate	134401-5
6	A6	0.2 M Ammonium formate		2.2 M Ammonium sulfate	134401-6
7	A7	0.18 M tri-Ammonium citrate		2.2 M Ammonium sulfate	134401-7
8	A8	0.2 M di-Ammonium phosphate		2.2 M Ammonium sulfate	134401-8
9	A9	0.2 M Ammonium iodide		2.2 M Ammonium sulfate	134401-9
10	A10	0.2 M Ammonium nitrate		2.2 M Ammonium sulfate	134401-10
11	A11	0.2 M di-Ammonium tartrate		2.2 M Ammonium sulfate	134401-11
12	A12	0.2 M Cadmium chloride		2.2 M Ammonium sulfate	134401-12
13	B1	0.2 M Cadmium sulfate		2.2 M Ammonium sulfate	134401-13
14	B2	0.2 M Cesium chloride		2.2 M Ammonium sulfate	134401-14
15	B3	0.2 M Cesium sulfate		2.2 M Ammonium sulfate	134401-15
16	B4	0.2 M Ammonium bromide		2.2 M Ammonium sulfate	134401-16
17	B5	0.2 M Lithium acetate		2.2 M Ammonium sulfate	134401-17
18	B6	0.2 M Lithium chloride		2.2 M Ammonium sulfate	134401-18
19	B7	0.2 M tri-Lithium citrate		2.2 M Ammonium sulfate	134401-19
20	B8	0.2 M Lithium nitrate		2.2 M Ammonium sulfate	134401-20
21	B9	0.2 M Lithium sulfate		2.2 M Ammonium sulfate	134401-21
22	B10	0.2 M Potassium acetate		2.2 M Ammonium sulfate	134401-22
23	B11	0.2 M Potassium bromide		2.2 M Ammonium sulfate	134401-23
24	B12	0.2 M Potassium chloride		2.2 M Ammonium sulfate	134401-24
25	C1	0.2 M tri-Potassium citrate		2.2 M Ammonium sulfate	134401-25
26	C2	0.2 M Potassium phosphate		2.2 M Ammonium sulfate	134401-26
27	C3	0.2 M Potassium fluoride		2.2 M Ammonium sulfate	134401-27
28	C4	0.2 M Potassium formate		2.2 M Ammonium sulfate	134401-28
29	C5	0.2 M di-Potassium phosphate		2.2 M Ammonium sulfate	134401-29
30	C6	0.2 M Potassium iodide		2.2 M Ammonium sulfate	134401-30
31	C7	0.2 M Potassium nitrate		2.2 M Ammonium sulfate	134401-31
32	C8	0.2 M K/Na tartrate		2.2 M Ammonium sulfate	134401-32
33	C9	0.2 M Potassium sulfate		2.2 M Ammonium sulfate	134401-33
34	C10	0.2 M Potassium thiocyanate		2.2 M Ammonium sulfate	134401-34
35	C11	0.2 M Sodium acetate		2.2 M Ammonium sulfate	134401-35
36	C12	0.2 M Sodium bromide		2.2 M Ammonium sulfate	134401-36
37	D1	0.2 M Sodium chloride		2.2 M Ammonium sulfate	134401-37
38	D2	0.2 M tri-Sodium citrate		2.2 M Ammonium sulfate	134401-38
39	D3	0.2 M Sodium phosphate		2.2 M Ammonium sulfate	134401-39
40	D4	0.2 M Sodium fluoride		2.2 M Ammonium sulfate	134401-40
41	D5	0.2 M Sodium formate		2.2 M Ammonium sulfate	134401-41
42	D6	0.2 M di-Sodium phosphate		2.2 M Ammonium sulfate	134401-42
43	D7	0.2 M Sodium iodide		2.2 M Ammonium sulfate	134401-43
44	D8	0.2 M Sodium malonate		2.2 M Ammonium sulfate	134401-44
45	D9	0.2 M Sodium nitrate		2.2 M Ammonium sulfate	134401-45
46	D10	0.2 M Sodium sulfate		2.2 M Ammonium sulfate	134401-46
47	D11	0.2 M di-Sodium tartrate		2.2 M Ammonium sulfate	134401-47
48	D12	0.2 M Sodium thiocyanate		2.2 M Ammonium sulfate	134401-48

#	Well	Salt	Buffer	Precipitant	100 ml Refill SKU
49	E1		0.1 M Citric acid pH 4.0	0.8 M Ammonium sulfate	134401-49
50	E2		0.1 M Citric acid pH 5.0	0.8 M Ammonium sulfate	134401-50
51	E3		0.1 M MES pH 6.0	0.8 M Ammonium sulfate	134401-51
52	E4		0.1 M HEPES pH 7.0	0.8 M Ammonium sulfate	134401-52
53	E5		0.1 M Tris pH 8.0	0.8 M Ammonium sulfate	134401-53
54	E6		0.1 M Bicine pH 9.0	0.8 M Ammonium sulfate	134401-54
55	E7		0.1 M Citric acid pH 4.0	1.6 M Ammonium sulfate	134401-55
56	E8		0.1 M Citric acid pH 5.0	1.6 M Ammonium sulfate	134401-56
57	E9		0.1 M MES pH 6.0	1.6 M Ammonium sulfate	134401-57
58	E10		0.1 M HEPES pH 7.0	1.6 M Ammonium sulfate	134401-58
59	E11		0.1 M Tris pH 8.0	1.6 M Ammonium sulfate	134401-59
60	E12		0.1 M Bicine pH 9.0	1.6 M Ammonium sulfate	134401-60
61	F1		0.1 M Citric acid pH 4.0	2.4 M Ammonium sulfate	134401-61
62	F2		0.1 M Citric acid pH 5.0	2.4 M Ammonium sulfate	134401-62
63	F3		0.1 M MES pH 6.0	2.4 M Ammonium sulfate	134401-63
64	F4		0.1 M HEPES pH 7.0	2.4 M Ammonium sulfate	134401-64
65	F5		0.1 M Tris pH 8.0	2.4 M Ammonium sulfate	134401-65
66	F6		0.1 M Bicine pH 9.0	2.4 M Ammonium sulfate	134401-66
67	F7		0.1 M Citric acid pH 4.0	3.2 M Ammonium sulfate	134401-67
68	F8		0.1 M Citric acid pH 5.0	3.2 M Ammonium sulfate	134401-68
69	F9		0.1 M MES pH 6.0	3.2 M Ammonium sulfate	134401-69
70	F10		0.1 M HEPES pH 7.0	3.2 M Ammonium sulfate	134401-70
71	F11		0.1 M Tris pH 8.0	3.2 M Ammonium sulfate	134401-71
72	F12		0.1 M Bicine pH 9.0	3.2 M Ammonium sulfate	134401-72
73	G1	0.1 M tri-Sodium citrate		0.5 M Ammonium sulfate; 1.0 M Lithium Sulfate	134401-73
74	G2			1.0 M Ammonium sulfate	134401-74
75	G3		0.1 M Sodium acetate pH 4.6	1.0 M Ammonium sulfate	134401-75
76	G4		0.1 M HEPES sodium salt pH 7.5	1.0 M Ammonium sulfate; 2% (w/v) PEG 400	134401-76
77	G5		0.1 M Tris-HCl pH 8.5	1.0 M Ammonium sulfate	134401-77
78	G6	0.05 M tri-Sodium citrate		1.2 M Ammonium sulfate; 3% (w/v) Isopropanol	134401-78
79	G7		0.1 M Tris-HCl pH 8.5	1.5 M Ammonium sulfate; 15% (w/v) Glycerol	134401-79
80	G8	0.5 M Lithium chloride		1.6 M Ammonium sulfate	134401-80
81	G9	1.0 M Lithium sulfate		1.6 M Ammonium sulfate	134401-81
82	G10	0.2 M Sodium chloride	0.1 M HEPES sodium salt pH 7.5	1.6 M Ammonium sulfate	134401-82
83	G11		0.1 M HEPES sodium salt pH 7.5	1.6 M Ammonium sulfate; 2% (w/v) PEG 1000	134401-83
84	G12		0.1 M MES sodium salt pH 6.5	1.8 M Ammonium sulfate	134401-84
85	H1	2.0 M Sodium chloride		2.0 M Ammonium sulfate	134401-85
86	H2		0.1 M Sodium acetate pH 4.6	2.0 M Ammonium sulfate	134401-86
87	H3		0.1 M MES sodium salt pH 6.5	2.0 M Ammonium sulfate; 5% (w/v) PEG 400	134401-87
88	H4		0.1 M Tris-HCl pH 8.5	2.0 M Ammonium sulfate	134401-88
89	H5			2.2 M Ammonium sulfate	134401-89
90	H6			2.2 M Ammonium sulfate; 20% (w/v) Glycerol	134401-90
91	H7	0.1 M tri-Sodium citrate		2.4 M Ammonium sulfate	134401-91
92	H8			3.0 M Ammonium sulfate; 1% (w/v) MPD	134401-92
93	H9			3.0 M Ammonium sulfate; 10% (w/v) Glycerol	134401-93
94	H10		0.1 M HEPES sodium salt pH 7.5	3.5 M Ammonium sulfate	134401-94
95	H11		0.1 M MES sodium salt pH 6.5	3.5 M Ammonium sulfate; 1% (w/v) MPD	134401-95
96	H12			3.5 M Ammonium sulfate	134401-96

Appendix II. BioRender's Publication License



49 Spadina Ave. Suite 200
Toronto ON M5V 2J1 Canada
www.biorender.com

Confirmation of Publication and Licensing Rights

October 23rd, 2023
Science Suite Inc.

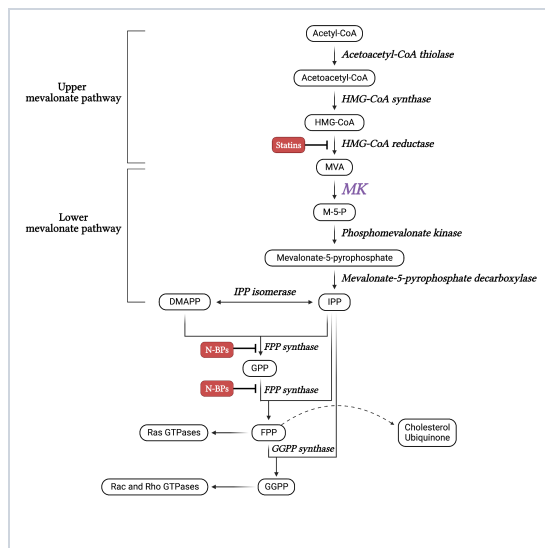
Subscription: Institution
Agreement number: ZC260CRJ3V
Journal name: M.Sc. Thesis

To whom this may concern,

This document is to confirm that Saman Salari has been granted a license to use the BioRender content, including icons, templates and other original artwork, appearing in the attached completed graphic pursuant to BioRender's [Academic License Terms](#). This license permits BioRender content to be sublicensed for use in journal publications.

All rights and ownership of BioRender content are reserved by BioRender. All completed graphics must be accompanied by the following citation: "Created with BioRender.com".

BioRender content included in the completed graphic is not licensed for any commercial uses beyond publication in a journal. For any commercial use of this figure, users may, if allowed, recreate it in BioRender under an Industry BioRender Plan.



For any questions regarding this document, or other questions about publishing with BioRender refer to our [BioRender Publication Guide](#), or contact BioRender Support at support@biorender.com.

Figure S1) Publication permission for Figure 1.

Confirmation of Publication and Licensing Rights

October 23rd, 2023
 Science Suite Inc.

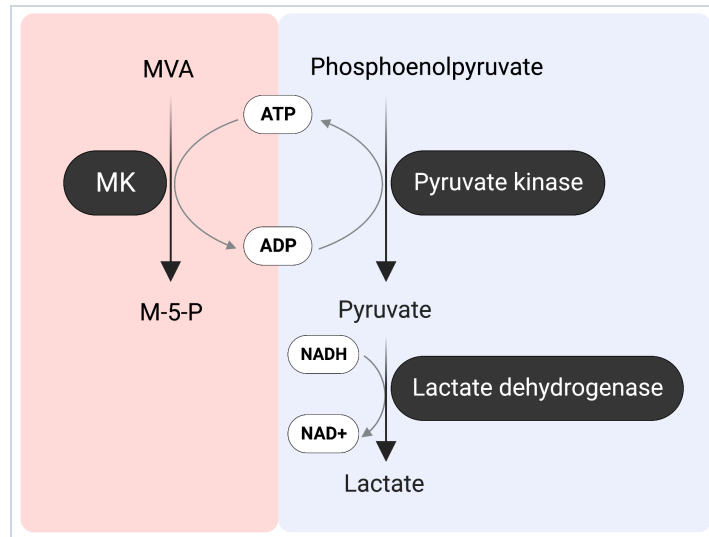
Subscription: Institution
Agreement number: NQ260CRL2J
Journal name: M.Sc. Thesis

To whom this may concern,

This document is to confirm that Saman Salari has been granted a license to use the BioRender content, including icons, templates and other original artwork, appearing in the attached completed graphic pursuant to BioRender's [Academic License Terms](#). This license permits BioRender content to be sublicensed for use in journal publications.

All rights and ownership of BioRender content are reserved by BioRender. All completed graphics must be accompanied by the following citation: "Created with BioRender.com".

BioRender content included in the completed graphic is not licensed for any commercial uses beyond publication in a journal. For any commercial use of this figure, users may, if allowed, recreate it in BioRender under an Industry BioRender Plan.



For any questions regarding this document, or other questions about publishing with BioRender refer to our [BioRender Publication Guide](#), or contact BioRender Support at support@biorender.com.

Figure S2) Publication permission for Figure 17.